Simulation of Materials - 2010 using TAMU SC Facilities

Tahir ÇAĞIN

Laboratory for Computational
Engineering of Nanomaterials and Devices

http://che.tamu.edu/orgs/groups/Cagin/

Artie McFerrin Department of Chemical Engineering

Texas A&M University

E-mail : cagin@che.tamu.edu

Summary

- Multiscale Modeling and Simulation of Materials
  - How we do
  - What we do

- Examples of Applications

  - Dynamic Response of Materials – Bedri Arman
  - Hydrogen Storage (MOFs, CNT nanostructures) – Mousumi Mani Biswas
  - Thermoelectrics - Alper Kinaci, Cem Sevik, Justin Haskins
  - Piezoelectrics and Ferroelectrics – Justin Haskins, Alper Kinaci
  - Magnetic Materials Alloys – Kristen Williams
  - Cyclic Peptide nanotubes (CPNT) – Jennifer Carvajal Diaz
  - Stress Corrosion Cracking in Fe based alloys – Hieu Pham
  - Nuclear Fuel materials – Cem Sevik
  - High Energy Density Materials – Oscar Ojeda
  - Nanocomposites – Arnab Chakrabarty, Jean Njorege, Carlos Silva
  - Thermal Transport – Alper Kinaci, Justin Haskins, Cem Sevik
  - Si-Ge nanocrystals, nanowires – Dundar Yilmaz, Cem Sevik

Acknowledgements

Financial Support: NSF, DARPA, ONR, ARO, DOE, & AFRL

NSF (ITR-ASE: stress corrosion)
NSF (IGERT): nanofluidics, SMA, CPNTs
NSF: fire retardant PNC's
DARPA (PROM: FE and TE materials)
ONR (Energetic Materials)
ONR (H-Pd under extreme conditions)
ARO (Energetic Materials)
AFRL (Thermo electrics)
AFRL (IED Sensing)
DOE (Nuclear Fuels)
DOE (Multiscale Modeling)
CONACyT (Domain walls in FE devices)
CONACyT (Dielectric Gate Stacks)
TAMU (Transport in bio-nano systems)
PIIF (H-storage systems)
TUBITAK (Si-nanocrystals)
TUBITAK (MSMA's)
PMMA thin film electronics

TAMU Super Computing Facility

ARMAN, HASKINS
CHAKRABARTY, KINACI, SEVIK
PHAM, SHIV, OJEDA, CAGIN
KAMANI, LIZAROZU
BISWAS, CARVAJAL, WILLIAMS, NJOREGE

Design/Characterization Through Modeling Paradigm

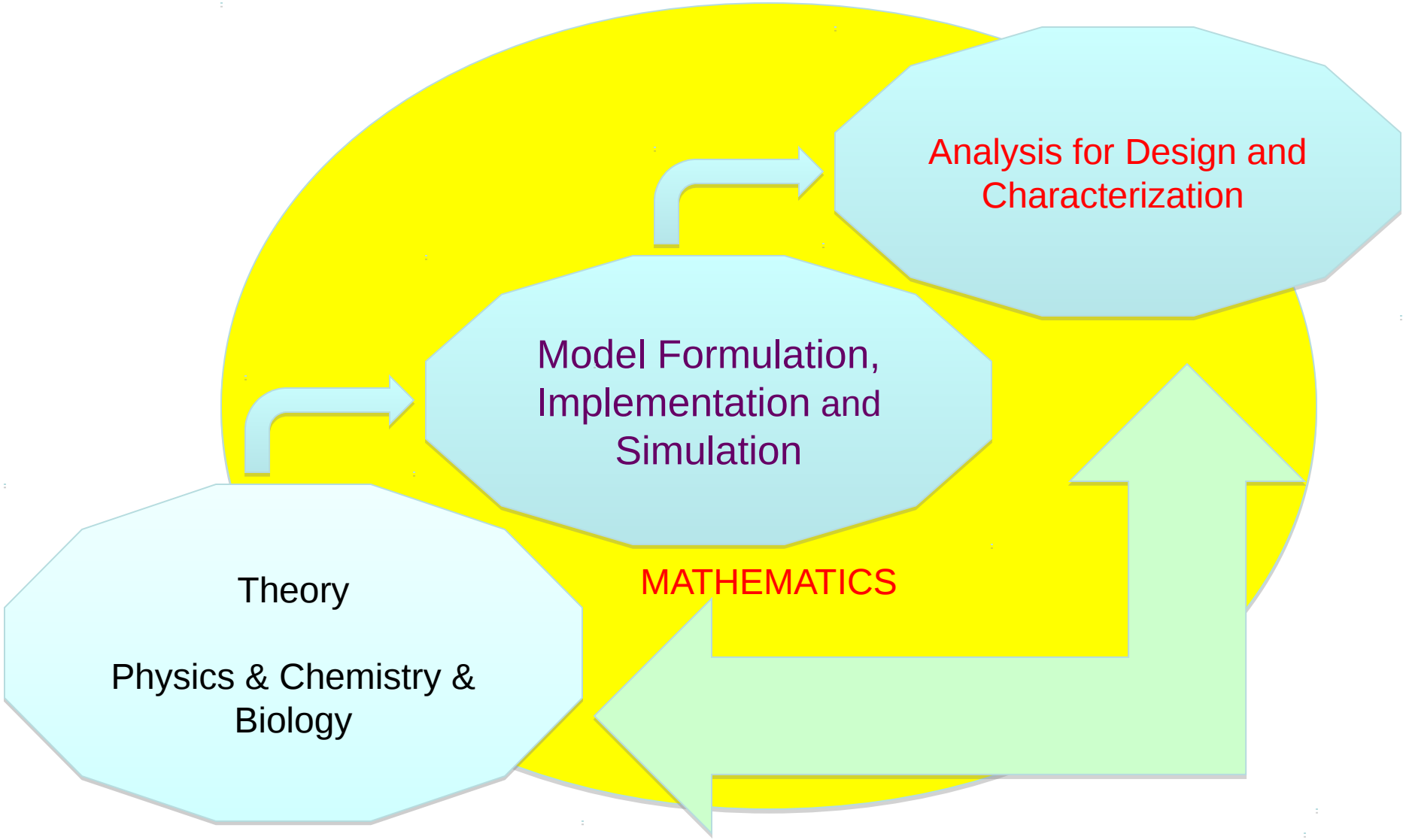

Multiscale Simulation and Modeling Hierarchy

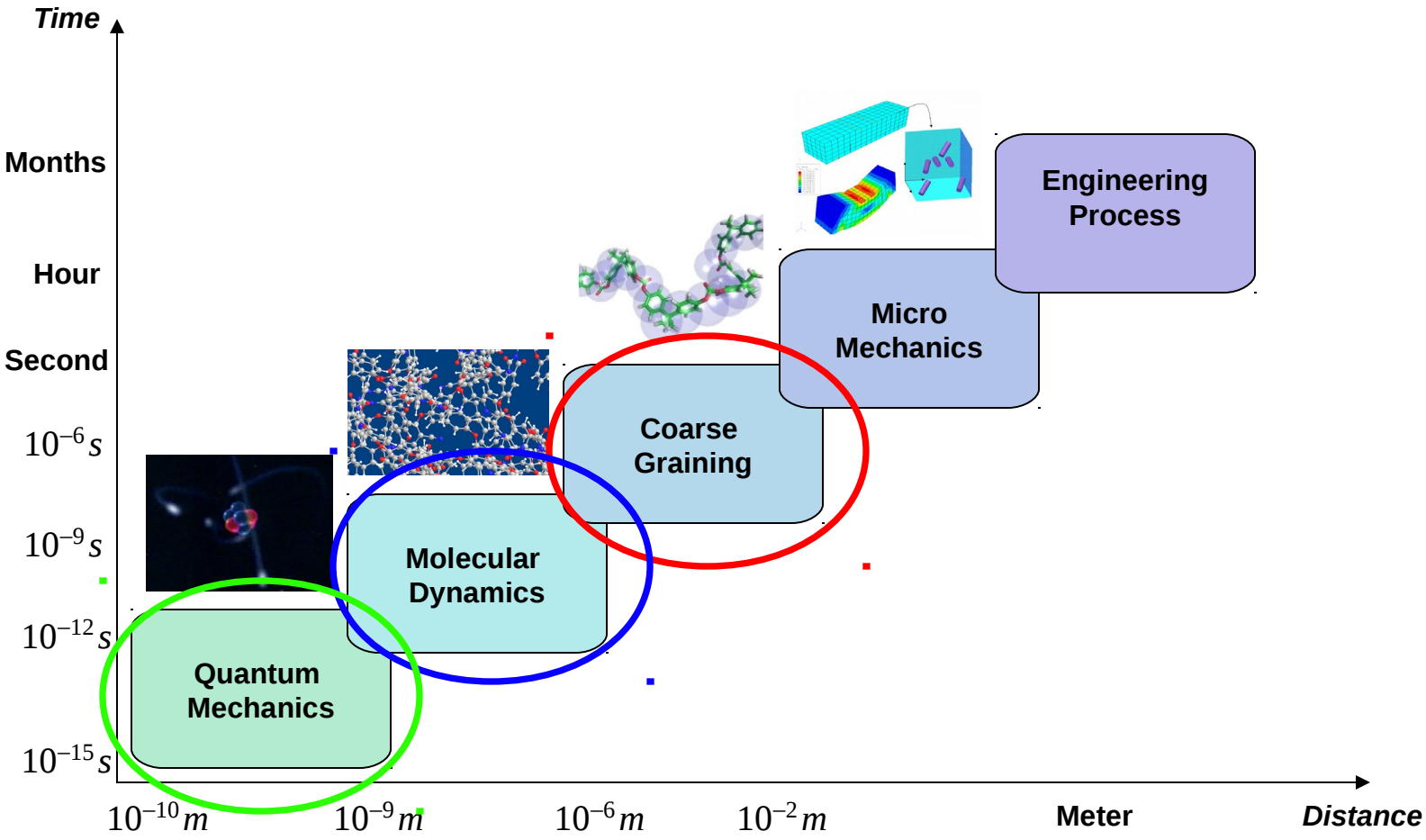

Dynamic Response of Metals and Metallic Glasses ($Cu_{46}Zr_{54}$) to shock loading

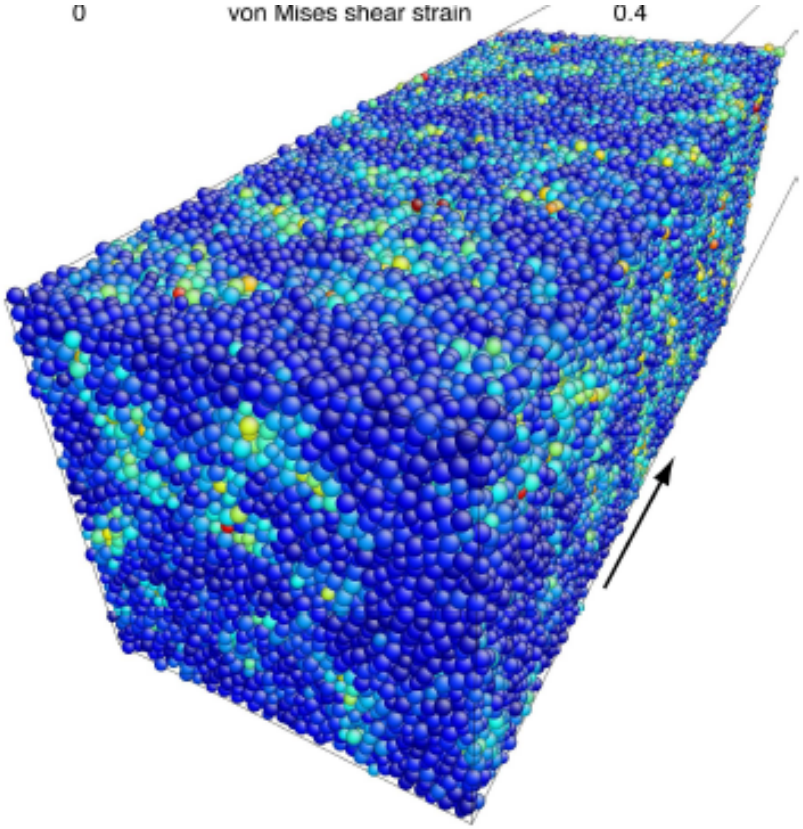

Arman, Luo, Gelman, Cagin, Phys. Rev. B, 2010.

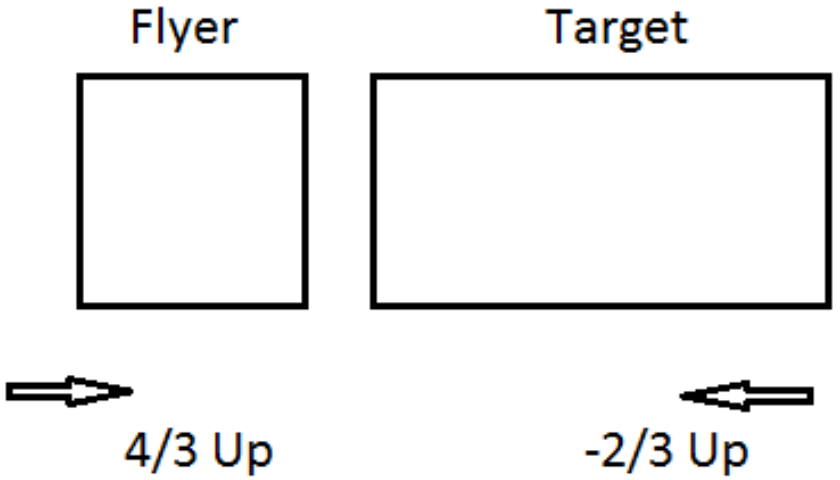

Planar shock-spall simulations are designed via following plate-target configuration

- 50-200 ps duration time
- Target size : 768000 atoms (flyer is half in size)
  - 8.4nm x 8.4nm x 200nm (4.2x4.2 and 16.8x16.8 were also examined)
  - A target length of 1.2 micron was also attempted

Void Nucleation

For Up= 0.5 km/s,
Viewed along the shock direction.

Atomeye program is used for visualization

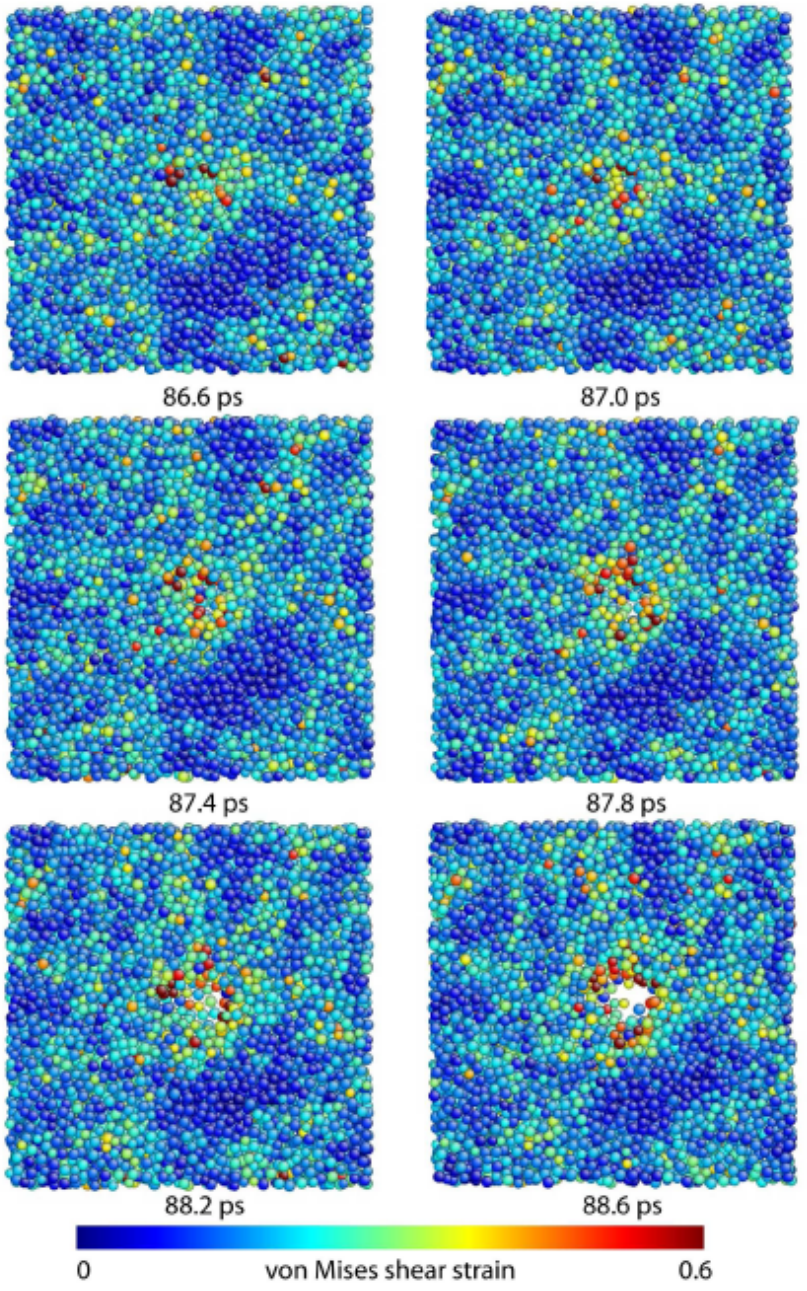

Shear strain at different shock loadings

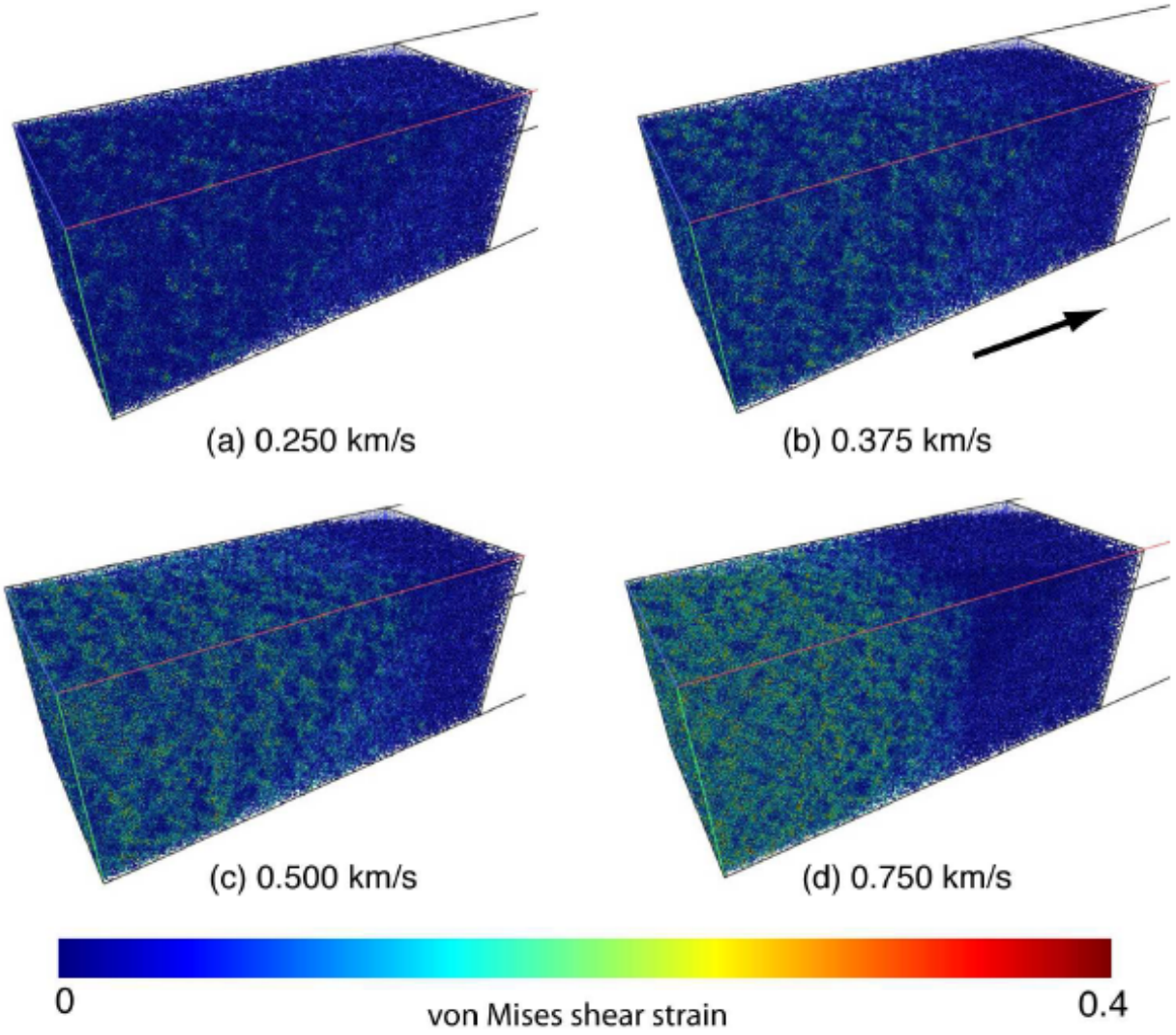

Rarefaction, Spallation in Pd with grain boundary

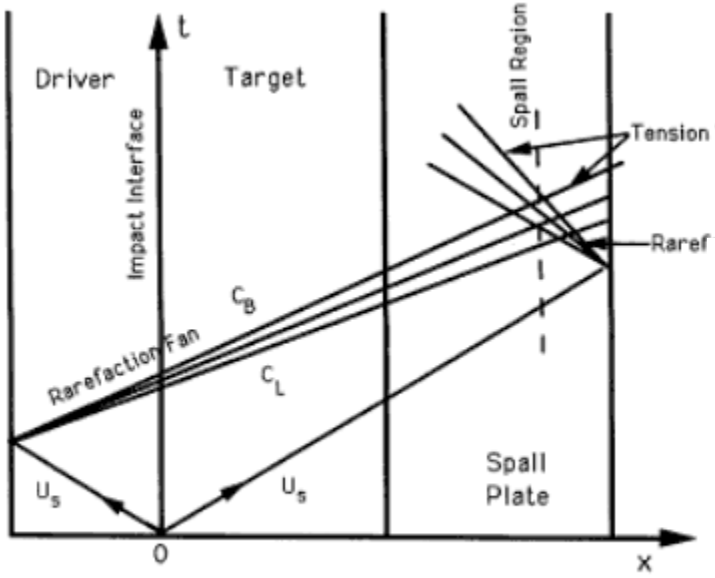

Figure 6.7. Lagrangian time–distance diagram of a symmetric in

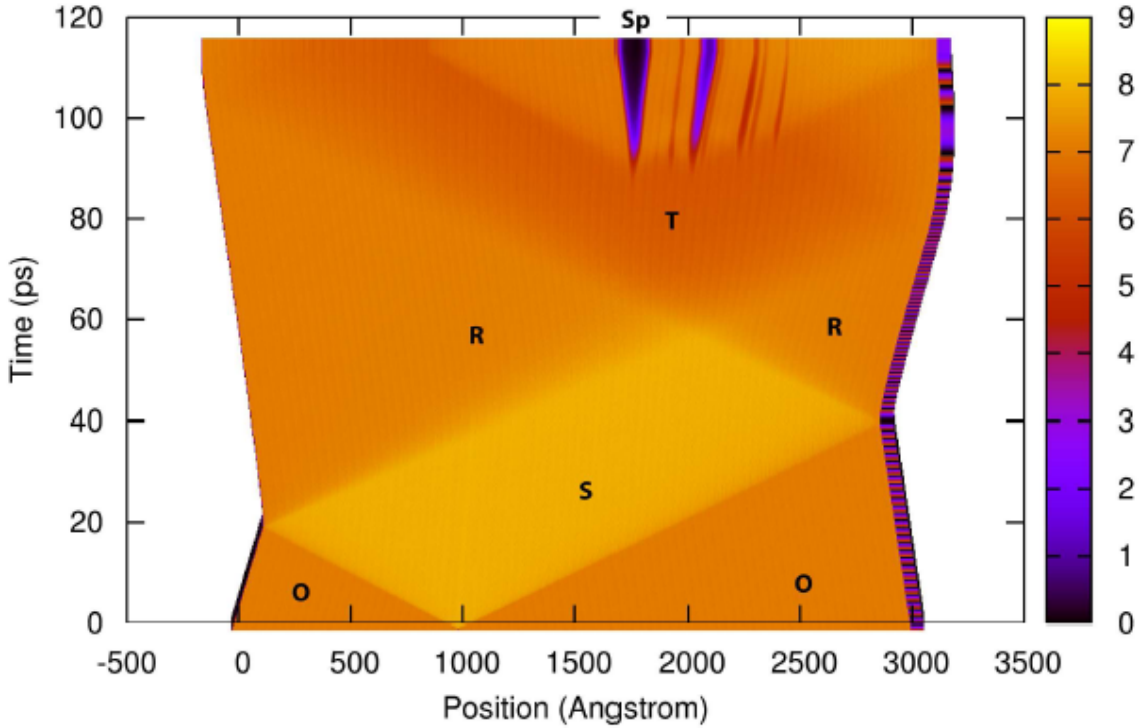

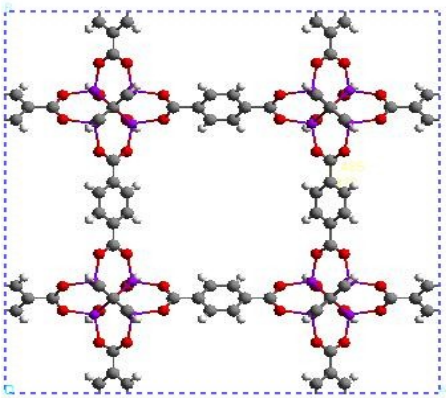

Loading at 100 MPa (298k)

Depressurize at 100 MPa

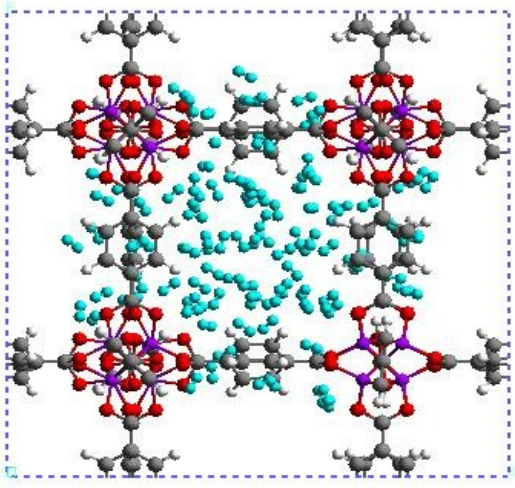

Unloading at 300 MPa (298k)

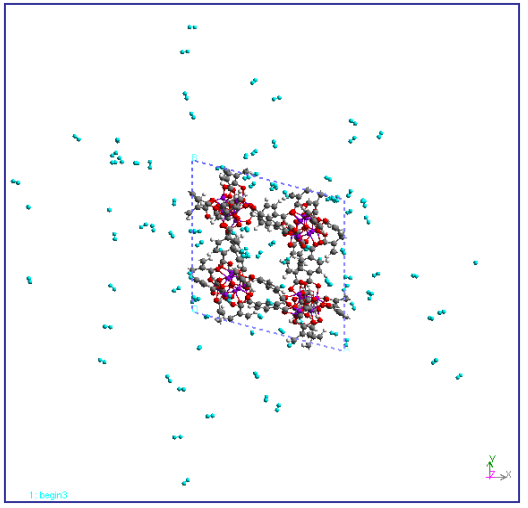

M. Mani-Biswas, T. Cagin, “Shape memory effect in MOFs”, to be submitted.

Simulation Studies on Carbon-Nanotube Scaffold for Hydrogen Storage

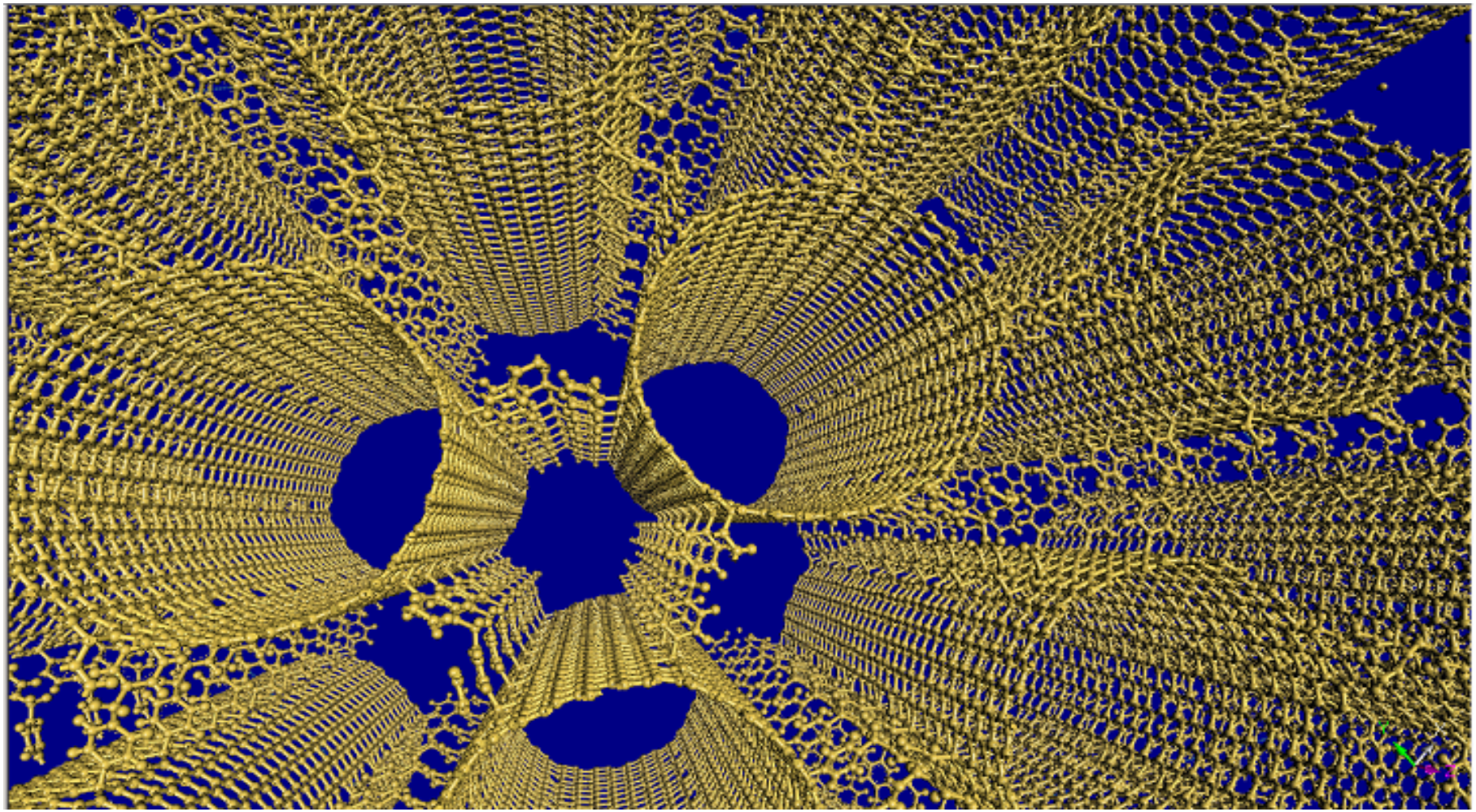

Mousumi Mani Biswas

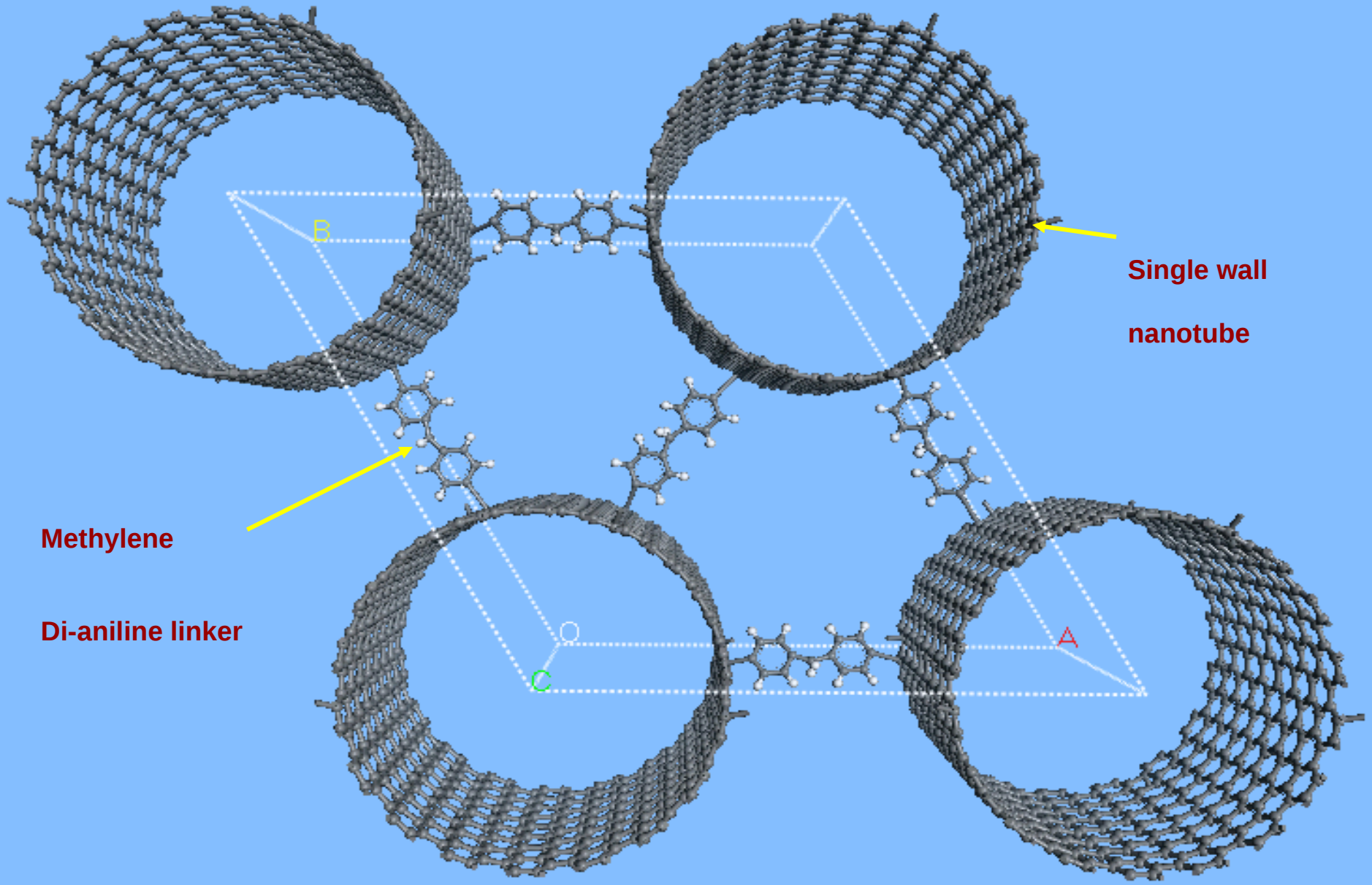
B
O
C
A
Single wall
nanotube
Methylene
Di-aniline linker

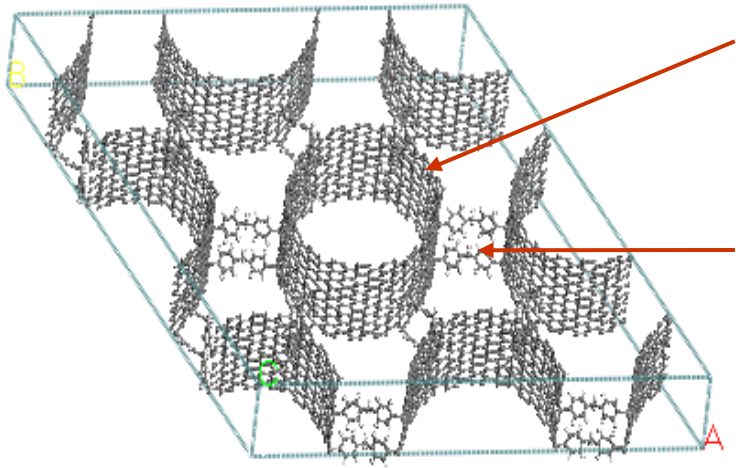

Tube

Linker

Construction of capped tube

Vary Tube diameter

Vary Cross linker periodicity

Sca

- (6,6), diameter 8.14 Å
- (9,9), diameter 12.20 Å
- (12,12), diameter 16.27 Å
- (15,15) diameter 20.34 Å
- (18, 18) diameter 24.4 Å,

Crosslinking agent, methylene di-aniline (length ~11 Å), attached after every

- 4 layers (4L), distance 9.8 Å,
- 7 layers (7L), distance 17.2 Å
- 9 layers (9L) distance 22.1 Å
- 12 layers (12L) distance 29.5 Å

of benzene rings (on the CNT) along the length of the tube.

Total Capacity

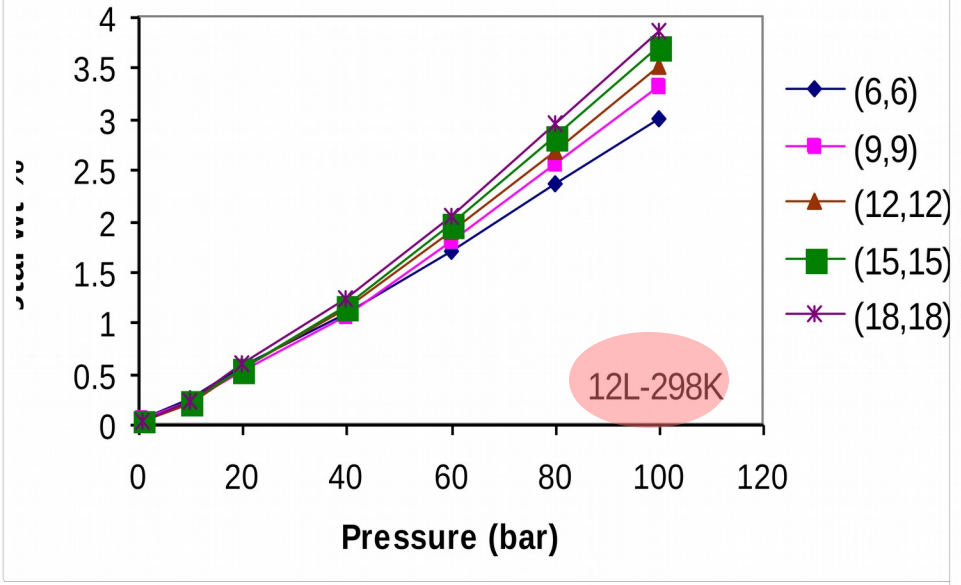

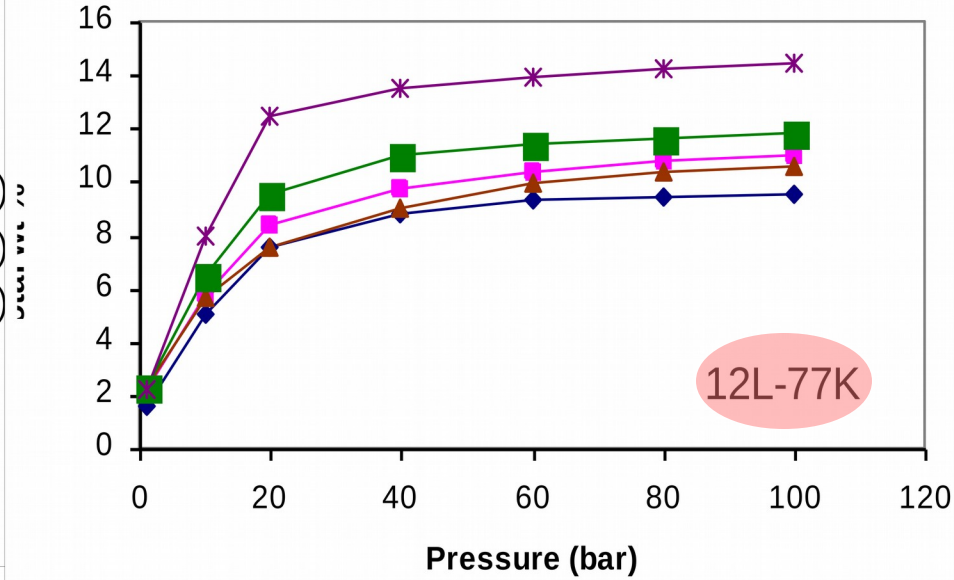

- **Maximum total capacity 3.86 wt% at 298K, 100 bar without reaching saturation and 14.4 wt% with (18,18), 12L scaffold, at 77 K,100 bar**

- **Sorption capacity at 77 K matches reported values by other researchers,**
  - ***Darkrim and Levesque*** **reported a total capacity of 11.2 wt% at 10 MPa (100 bar), 77 K with tube diameter 22 Å and inter-tube spacing of 11 Å.**

- **Capacity of Ar filled tubes (closed tubes) is half of open tubes.**

Darkrim, F.; Levesque, D. *J. Phys. Chem. B* **2000** 104, 6773-6776

Empty Scaffold- side view

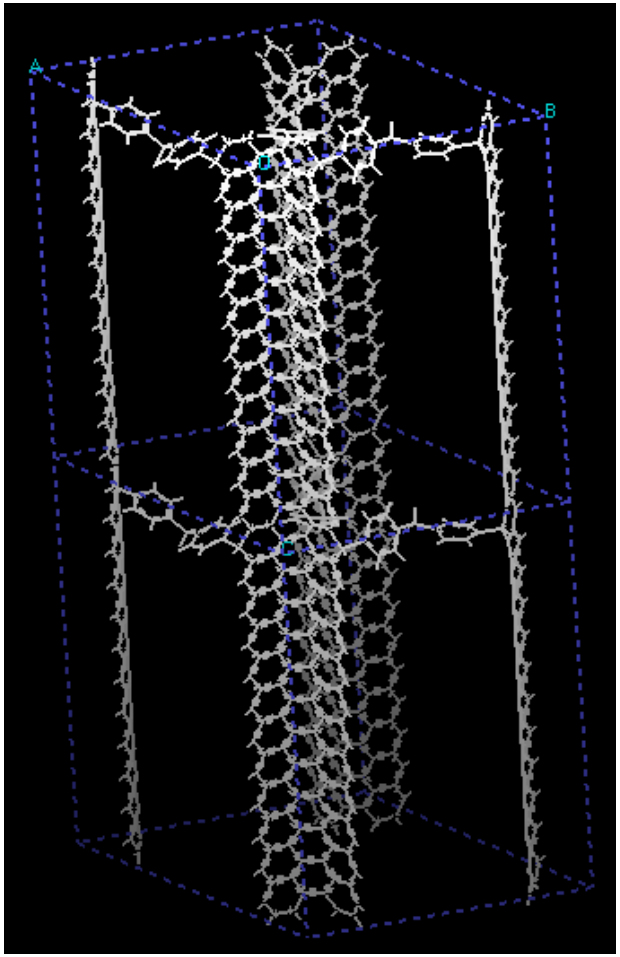

(6,6) 12L, 77K

Scaffold- Top view

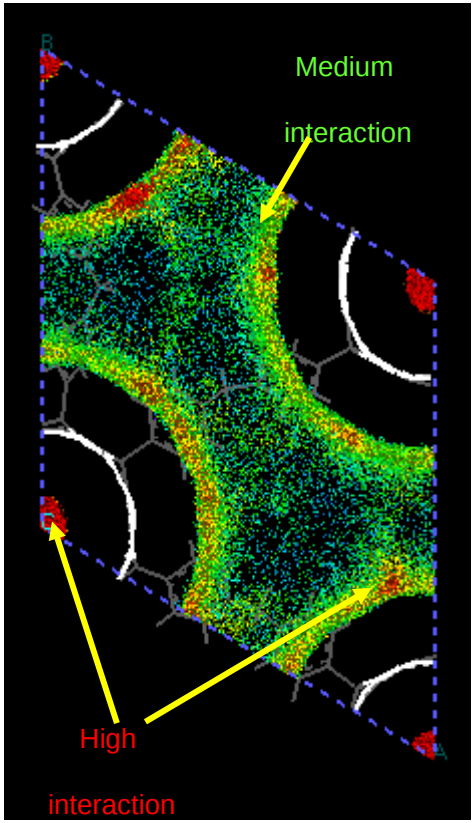

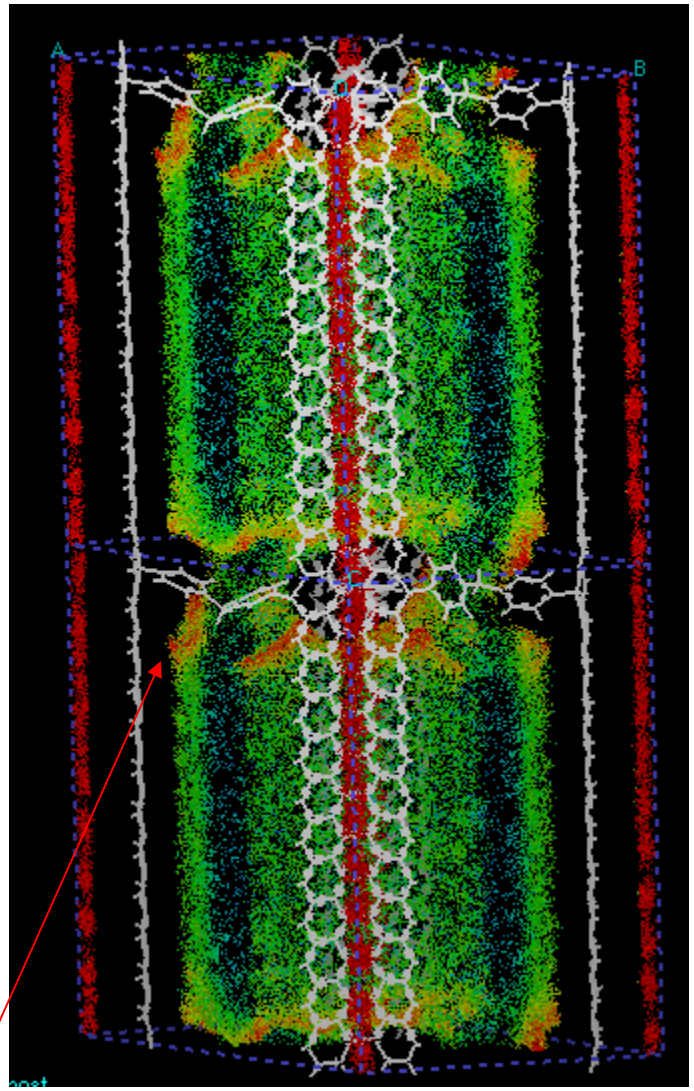

High Interaction

near the linker &

inside tube wall

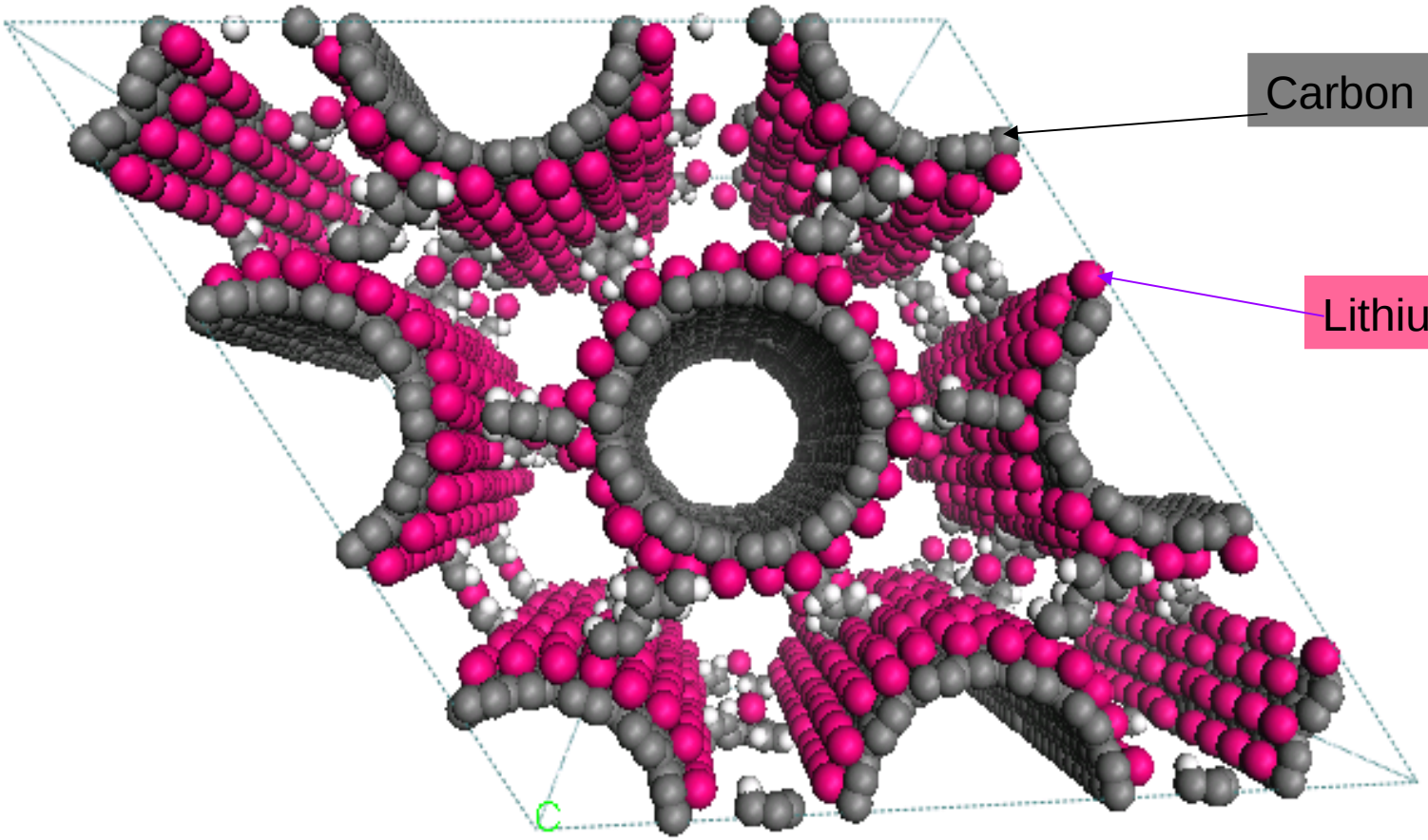

Li has almost vertical alignment along the tube wall, occupying the center point of the benzene ring (similar to the observation by other researchers)

Tubes are charged. Some lithium attached on the linker also.

298 K w/o Li

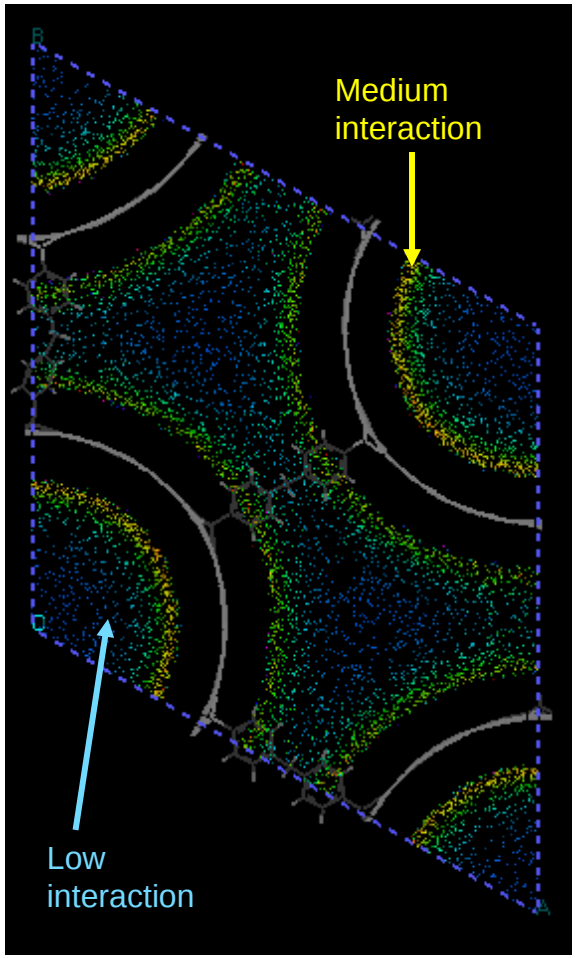

298 K with Li

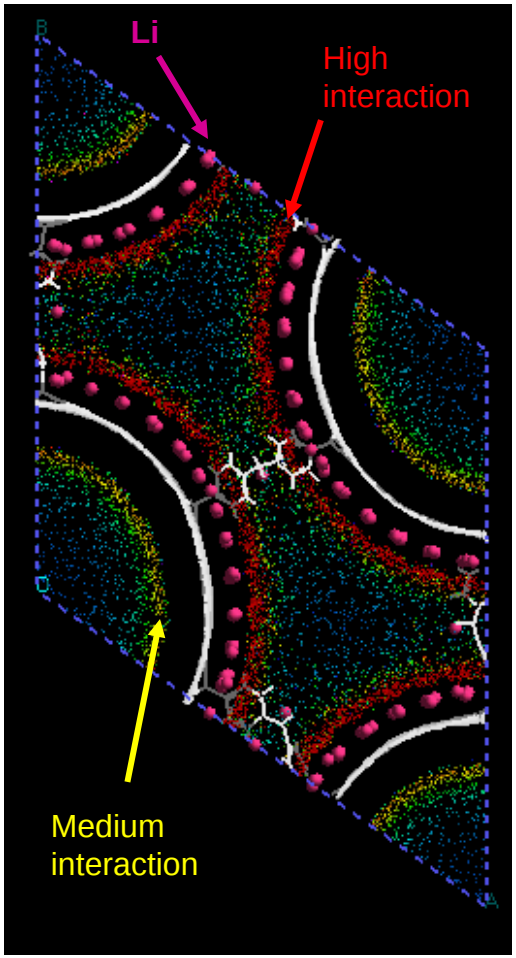

243 K with Li

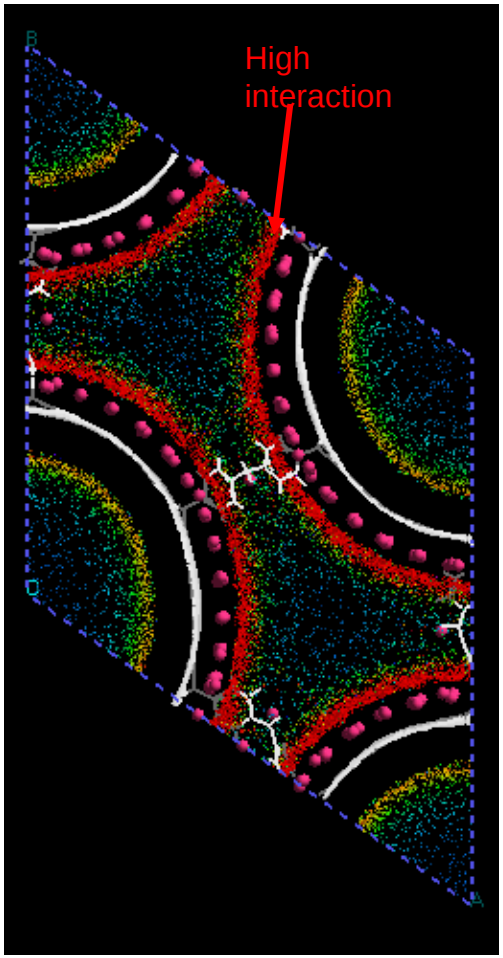

Thickness of high interaction zone increases in presence of Li^{+1}

Metal Organic Framework (MOF) for High Capacity Hydrogen Storage and Delivery

M. Mani Biswas, T. Cagin

- Crystalline material
  - Metal oxide clusters at vertexes,
  - Connected by organic linkers.
- Porous, large surface area (2500 - 5000 m^2/gm)
- Low density (0.59 gm/cc)

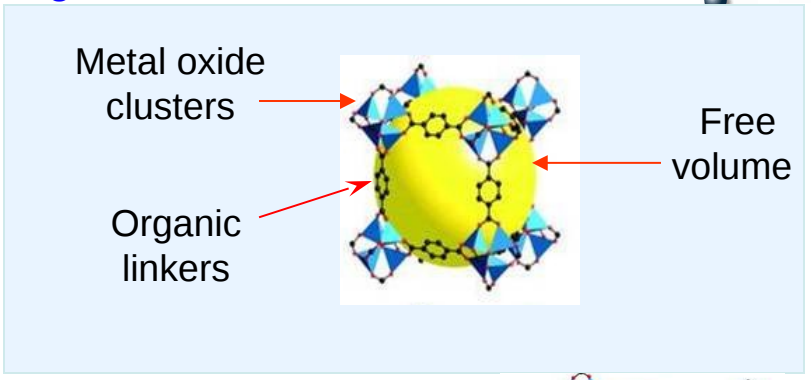

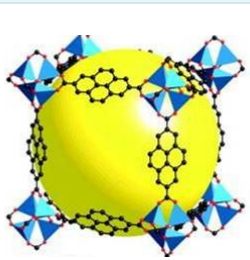

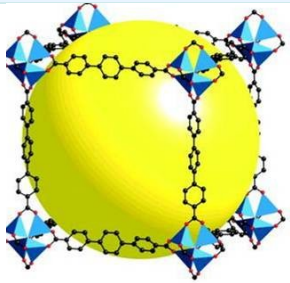

- Crystals can be designed
  - Geometry, pore size can be varied (3.8 - 30 Å)
  - Linker molecule of different chemistry can be chosen

- Selective storage of guest molecule inside free volume
  - Hydrogen gas storage, gas separation
  - Drug delivery vehicle
- Designable property
  - Catalysis, molecular detection

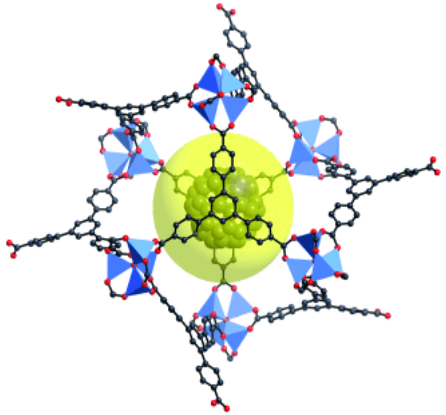

Ref: Li, H.; Eddaoudi, M.; O.Keeffe, M.; Yaghi, O. M., (1999) Design and synthesis of an exceptionally stable and highly porous metal-organic framework, *Nature*, 402, p. 276.

Theoretical Investigation using Classical MD simulations and Quantum Level calculation
- properties of Metal Organic Frameworks (MOF) for efficient hydrogen storage and delivery

System Integration

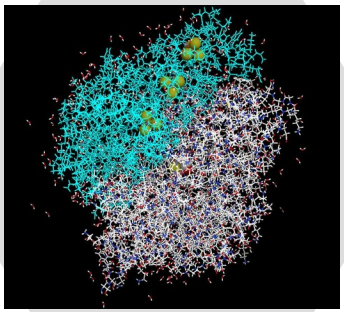

Study Hydrogen generation from renewable sources- Biological

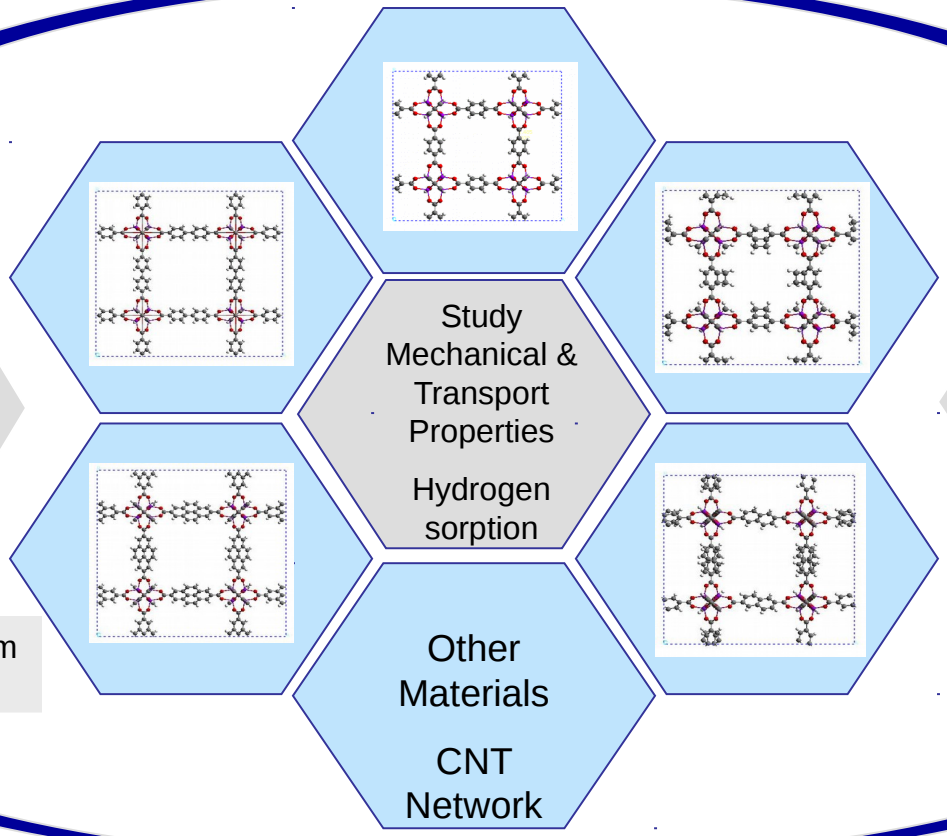

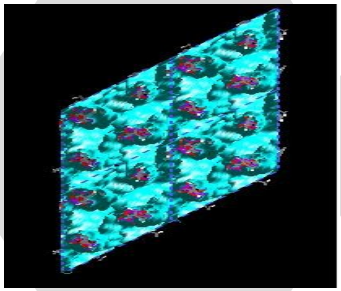

Build a device for hydrogen delivery to fuel cell

System Integration

Ferroelectrics & Piezoelectrics

Domain Wall: Interface of polarization domains

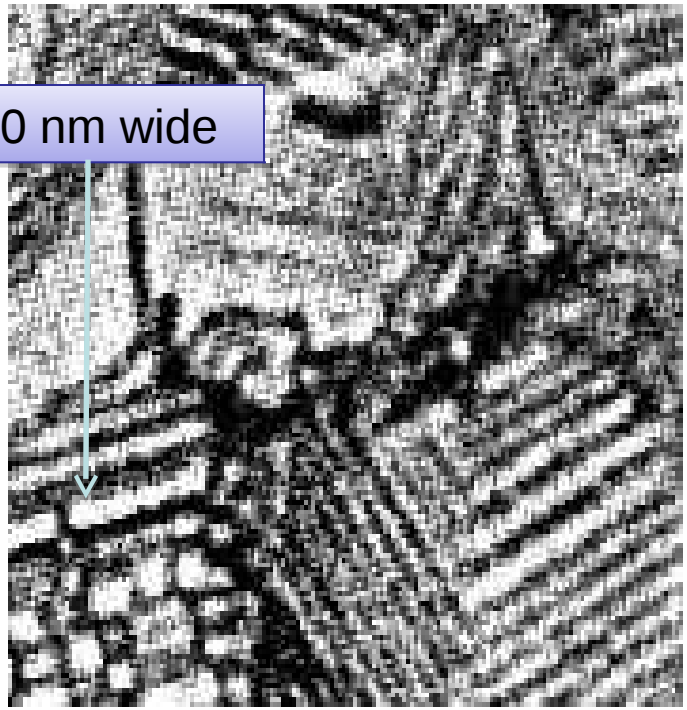

http://www.materials.leeds.ac.uk/luec/ActMats/Domain2.jpg

- Determine piezoelectric response and macroscopic polarization
- Fatigue switchable polarization
- Used in many applications
  - RAM
  - Actuators
  - Transducers
  - Sensors

Zhang, Cagin, Goddard, PNAS 103, 14695 (2006); Cagin et al, CMES 24, 215 (2008); Majdoub, Sharma, Cagin, PRB 78, 12407 (2008); PRB 77, 125424 (2008)
J. Haskins, A. Kinaci,T. Cagin in progress.

Simulations excel in investigating nanostructures and the origin of bulk properties.

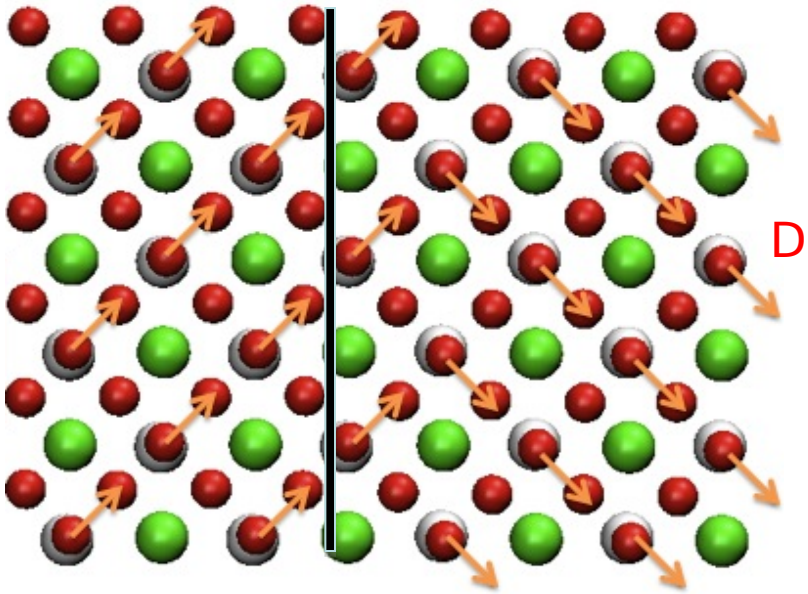

Domain Walls

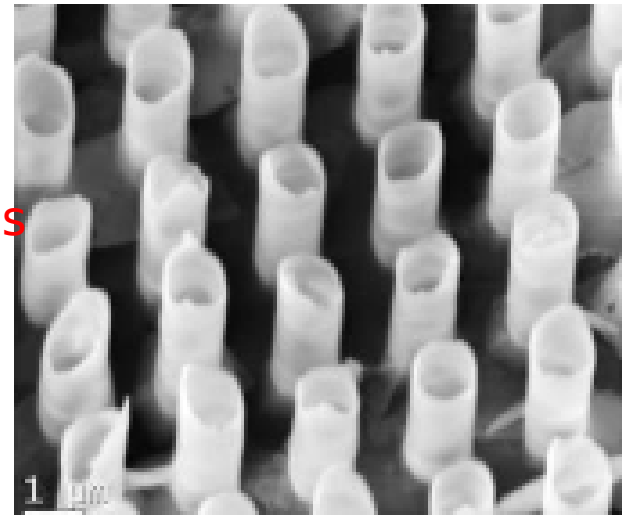

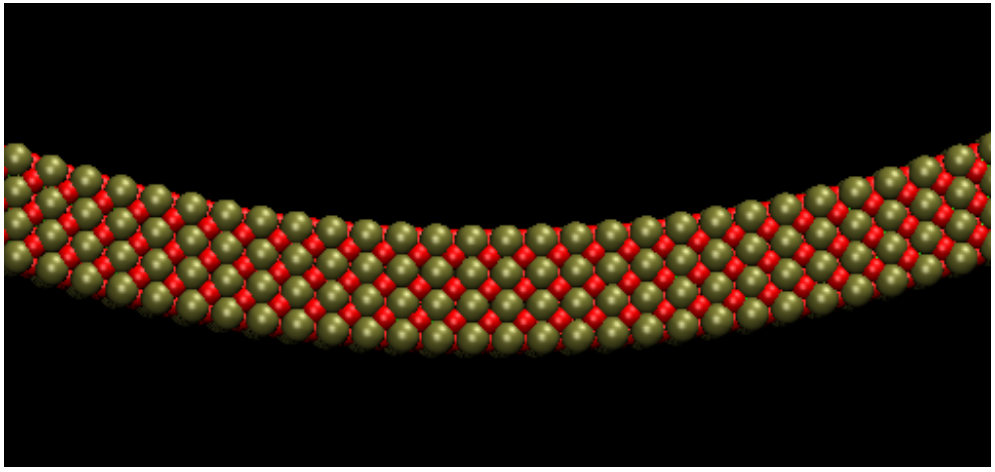

PZT nanotubes for memory devices

Nonlinearly strained cantilever polarization enhancement

Temperature behavior of PZT calculated by polarizable

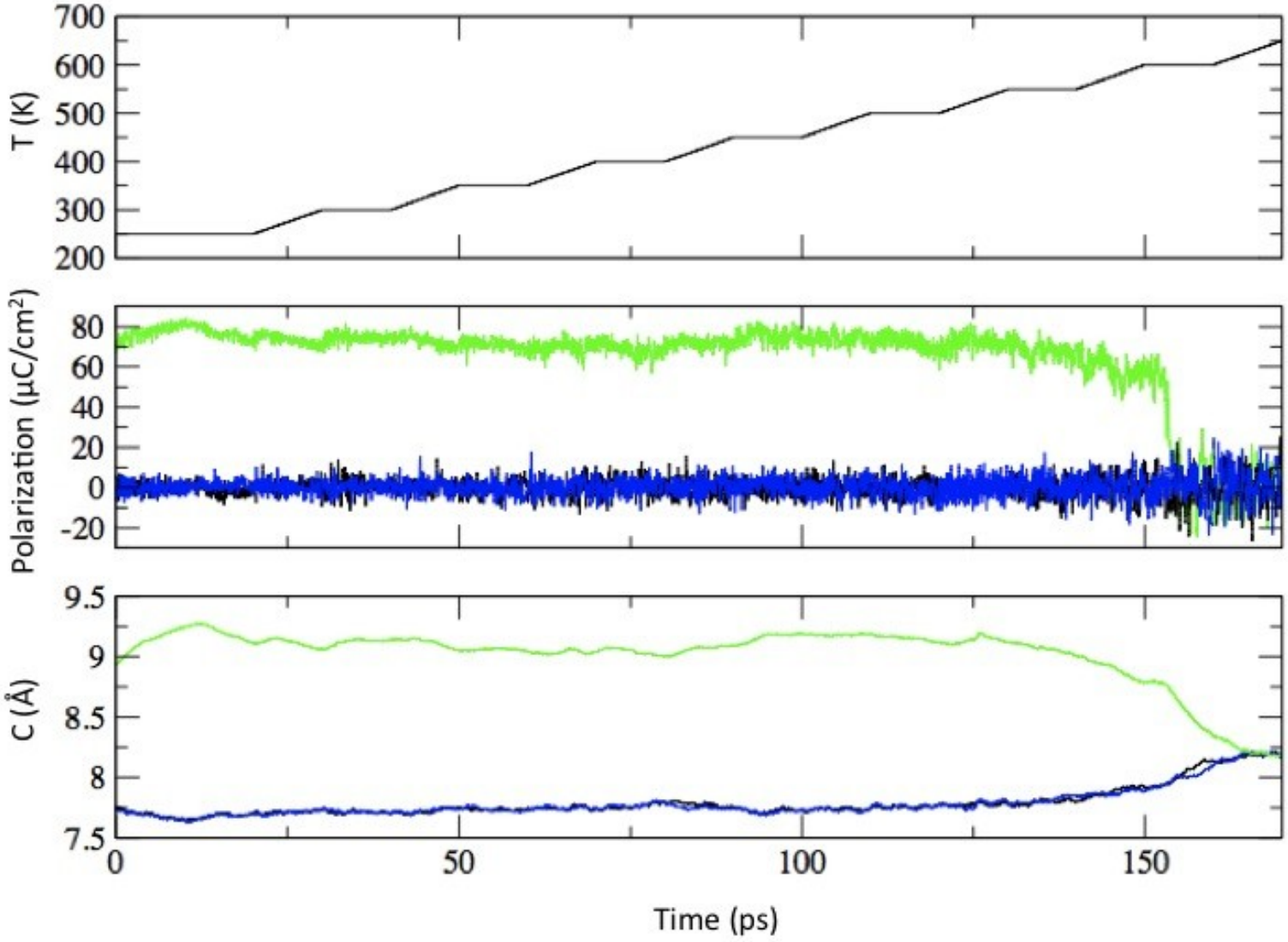

Hysteresis behavior of PT and PZT.

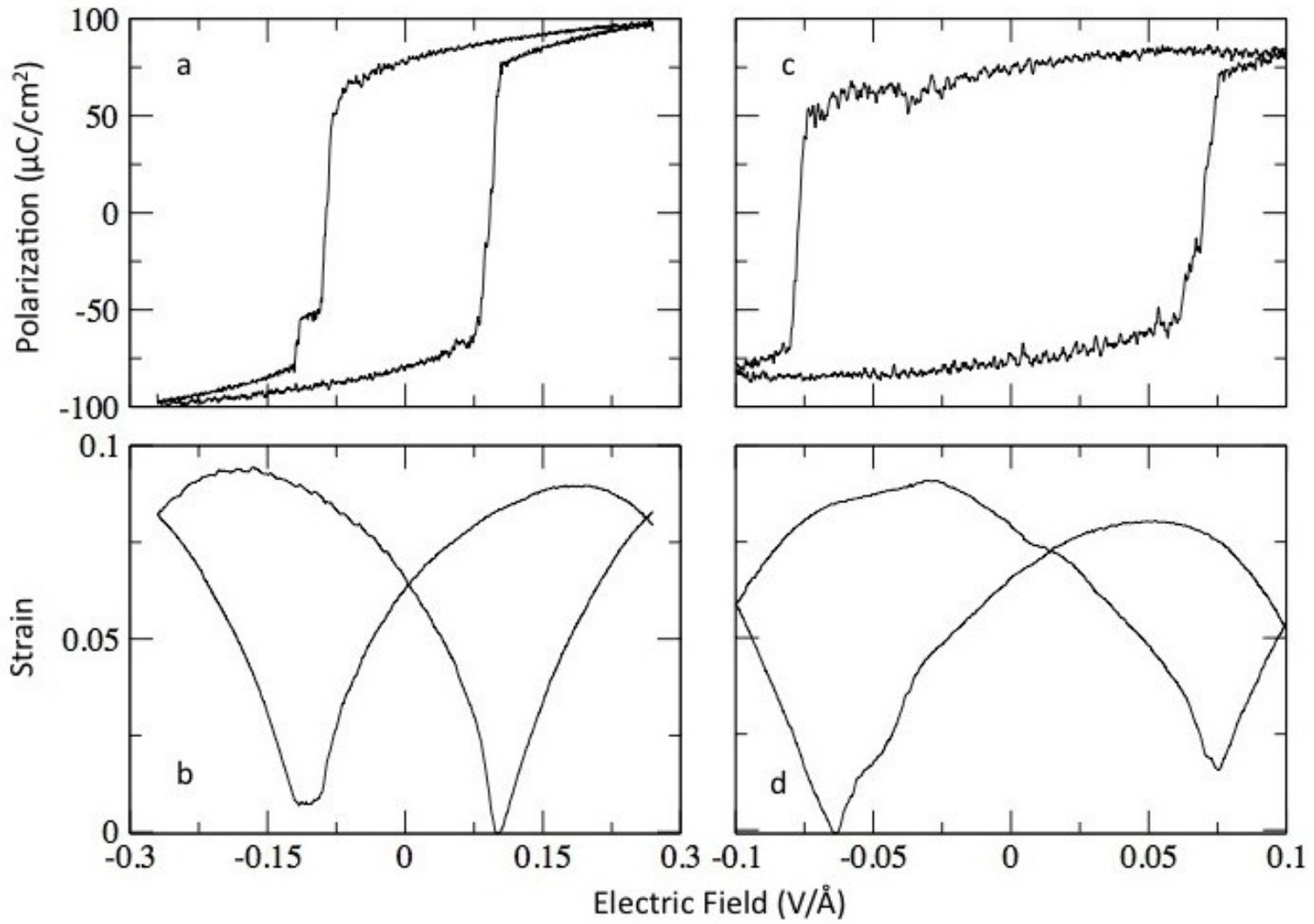

Triangle field of 1 GHz with maximum strength of 0.27 V/Å .

The simulations shows characteristic ferroelectric hysteresis behavior.

Stability and Optimization

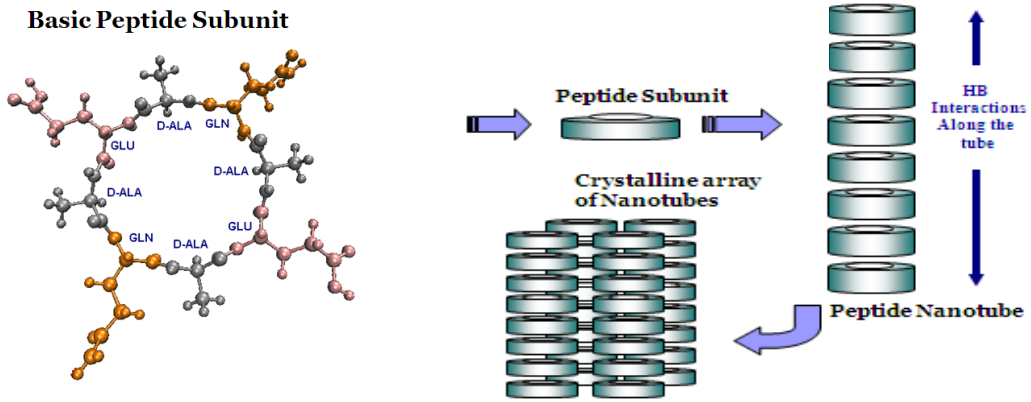

Crystalline nanotubes

8-Peptide System

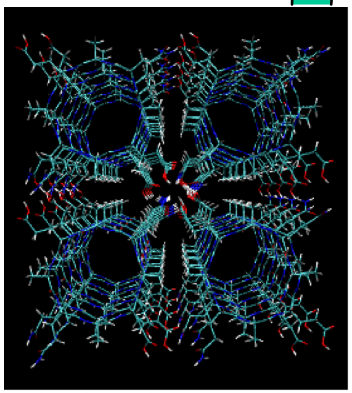

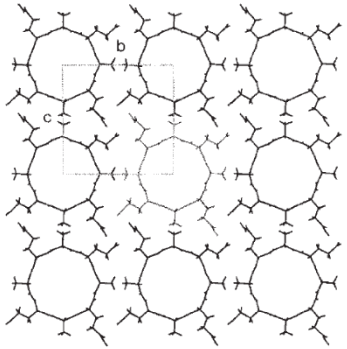

Name	Exp.	Sim.
a	9.5 A	9.6 A
b	15.1 A	15.3 A
c	15.1 A	15.1 A

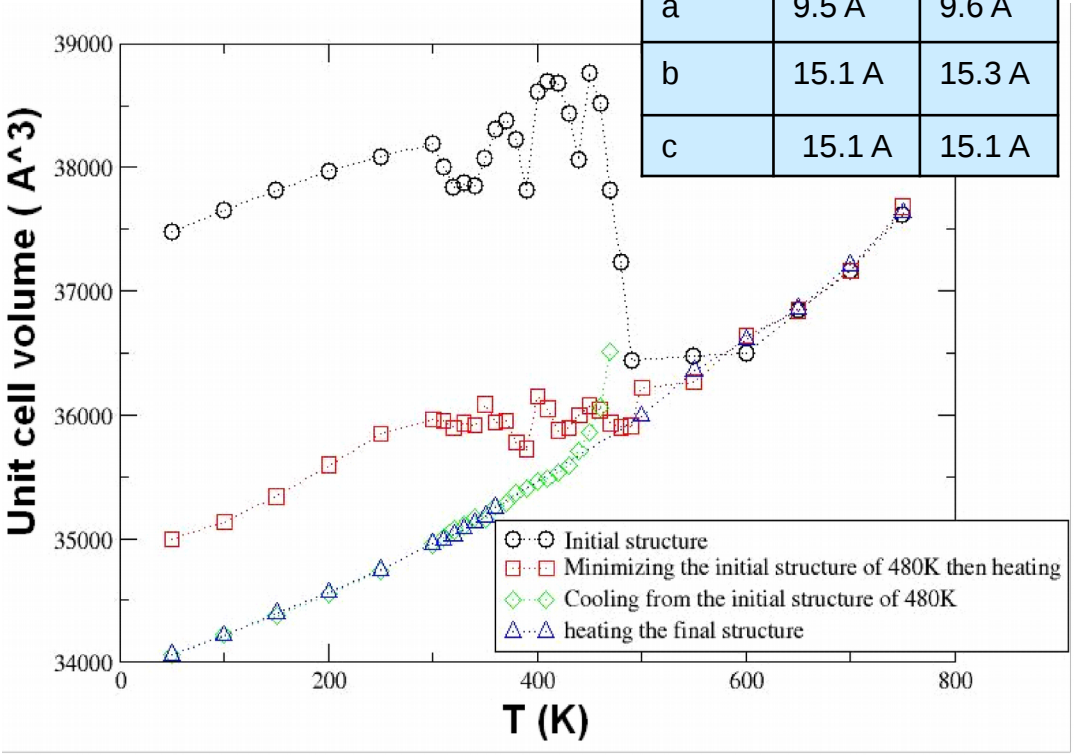

12-Peptide System

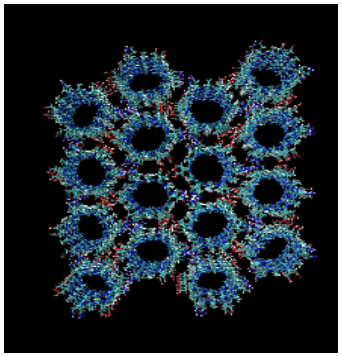

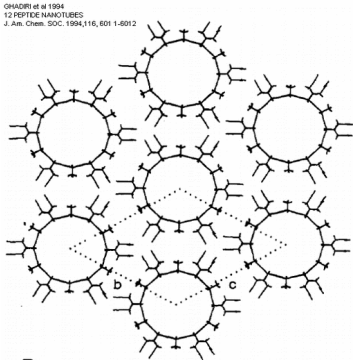

Transport Properties

Diffusion of water in Peptide Nanotubes is faster compared with equivalent diameters of CNTS.

Self Diffusion Coeficient

$$\left\langle (x(t+\Delta t)-x(t))^2 \right\rangle = 6*D*t$$

Einstein's Relationship

DETAILS
From the analysis of curves of mean square displacement along axial direction.

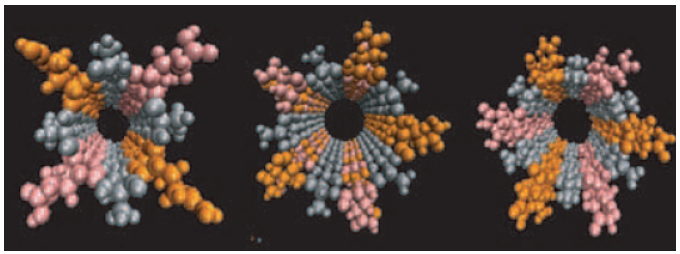

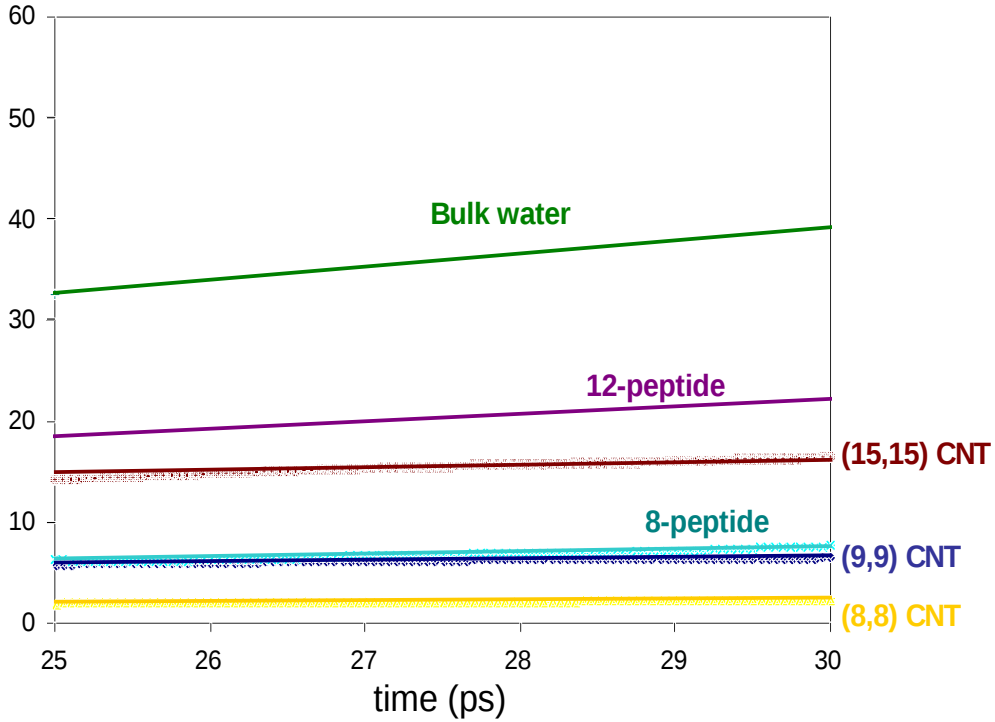

System	Diameter (A)	Diff. coeff. (calc) cm^2/s $(1*10^5)$
Bulk water	—	2.17
12-peptide	14	1.23
(15,15) CNT	15	0.41
8-peptide	8.8	0.41
(9,9) CNT	8.6	0.25
(8,8) CNT	7.2	0.13

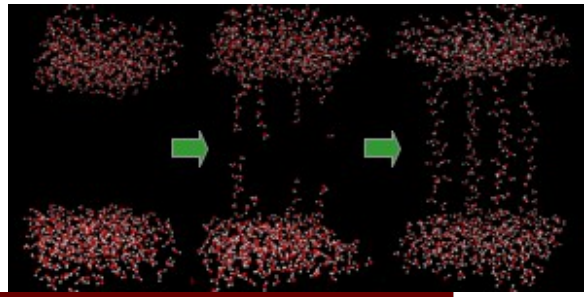

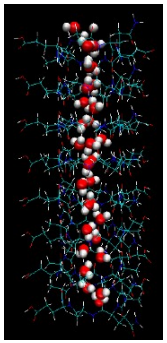

Mechanical Properties

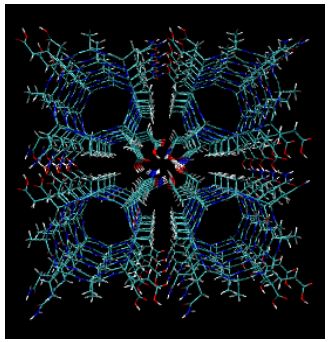

SIDE CHAIN- SIDE CHAIN INTERTUBULAR HYDROPHOBIC INTERACTIONS

HYDROGEN BONDING INTERACTION ALONG THE NANOTUBES

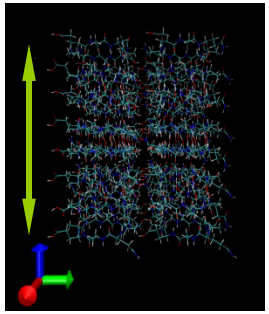

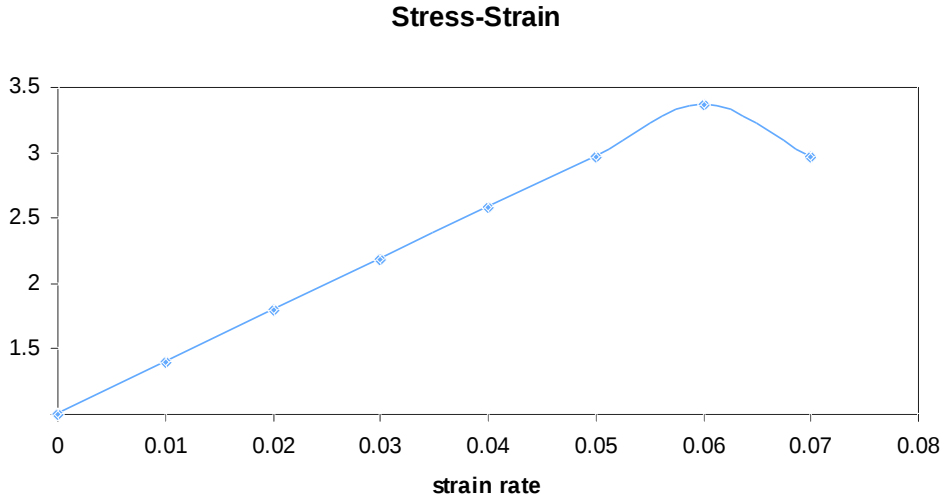

$$\Delta E = \frac{Vo}{2}\sum C_{IJ}\eta_I\eta_J + \frac{Vo}{6}\sum C_{IJK}\eta_I\eta_J\eta_K$$

Anisotropic Isothermal Elastic Constants

Cij	value(Gpa)	Cij	value(Gpa)
C11	8.09	C66	0.77
C22	10.16	C12	6.56
C33	19.65	C13	9.56
C44	1.23	C14	0.57
C55	1.23	C23	9.59

Experimental Young Modulus reported for Peptide Nanotubes :19GPa. *Self-Assembled Peptide Nanotubes Are Uniquely Rigid Bioinspired Supramolecular Structures. Nano Lett., 2005, 5 (7), pp 1343 ≦ 1346*

CPNTs as Artificial Ion Channels

Ion Transport in presence of Electric Field

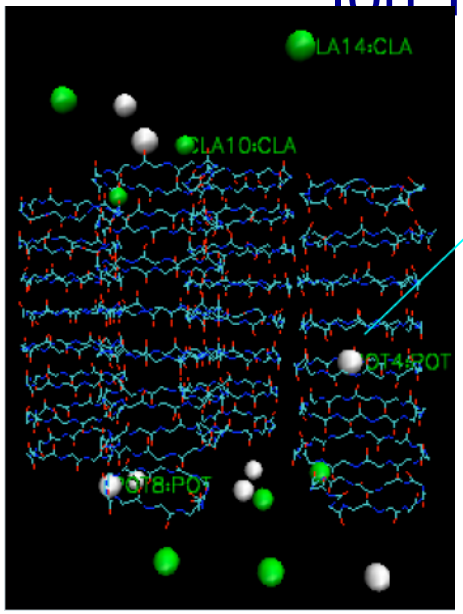

K+ ions inside the nanotube

Selectivity for cations was observed in the CPNT channel.

Simulation Details:

CPNT membrane was solvated and ionized with 0.5M of KCL and 0.5M NaCl respectively.
Minimization, Heating, NPT dynamics (equilibration)
NVT simulation at equilibrated system under effect of E field
Different Electric Fields were applied along z direction.
E= 0V/nm. 0.1 V/nm, 0.2 V/nm. 0.3 V/nm, 0.4 V/nm, 0.5 V/nm
12-peptide and 10-peptide channels were studied

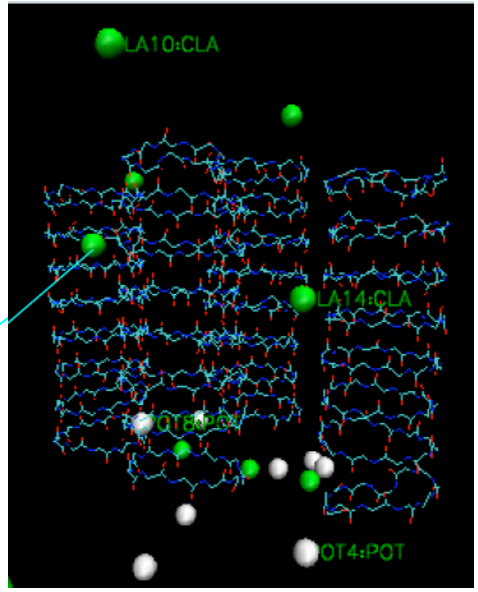

Cl- ions between the nanotubes

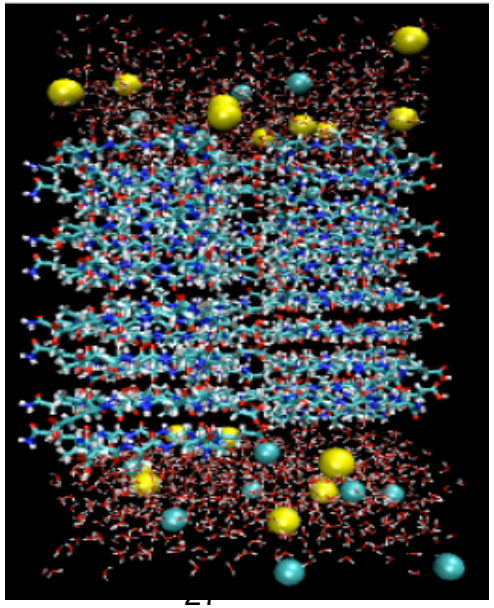

Preliminary Results

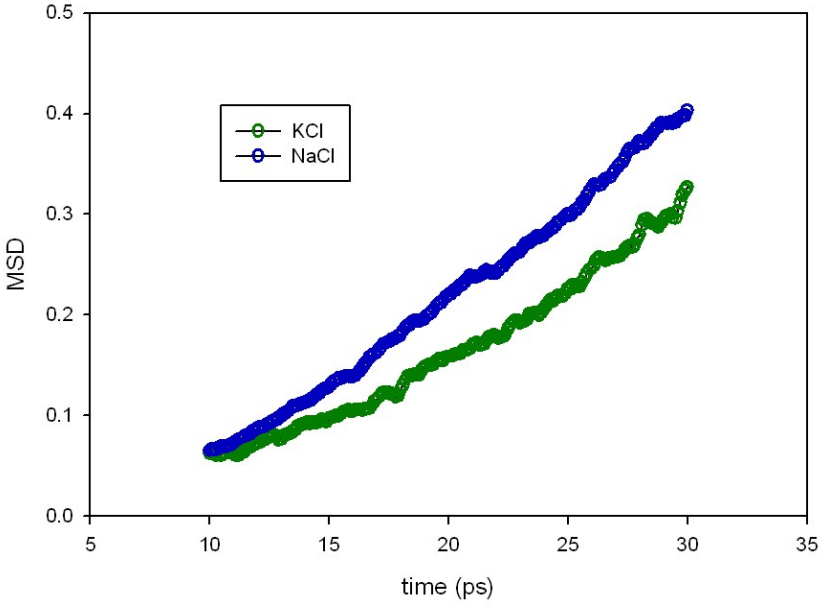

Comparison of Diffusion Coefficients

Ion	Diffusion Coeff. [m^2/s]
K+	0.07×10^{-11}
Na+	0.09×10^{-11}

Comparison in radial distribution function peaks and Diffusion coefficients was in good agreement with ion transport in similar ion channels (1).

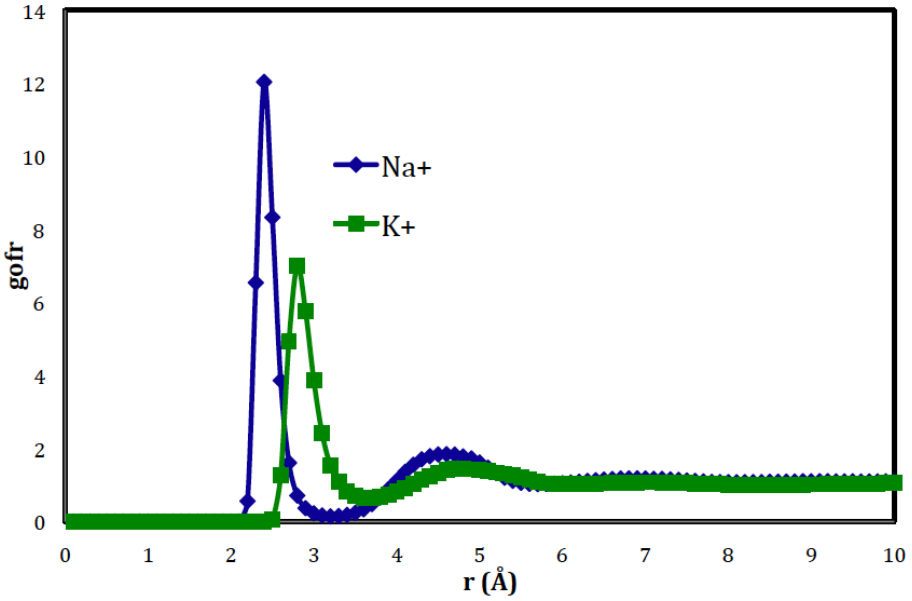

(1) Hu, Z. Q. & Jiang, J. W. Biophys J 95, 4148-4156 (2008).

Investigations of Magnetic Materials using TAMU Supercomputing Facilities

Grad Student

Kris Williams

Faculty

Tahir Çağin, CHEN

Ibrahim Karaman, MEEN

Jairo Sinova, PHYS

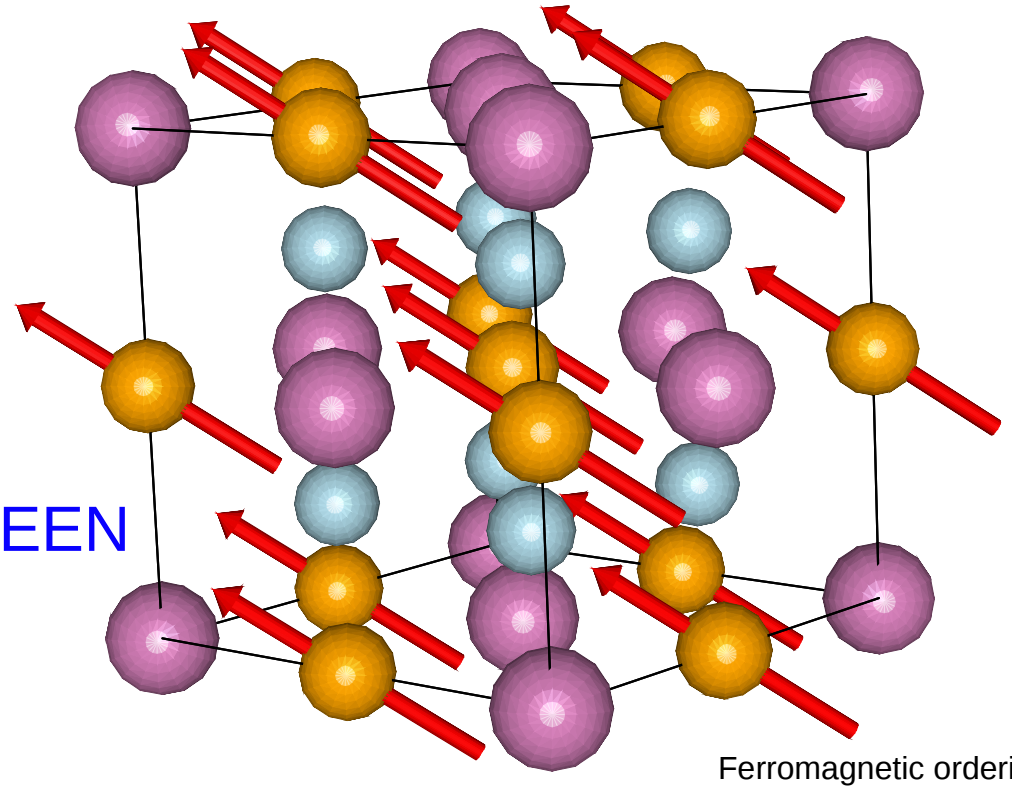

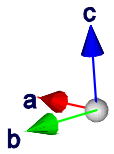

Ferromagnetic ordering in $L2_1$ Ni_2MnIn. Calculated with VASP on **hydra**. Image rendered with VESTA.

Case Study #1
Magnetic Shape Memory Alloys

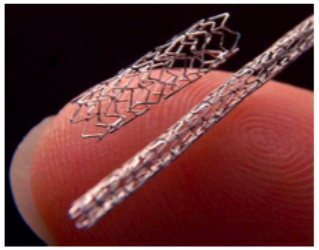
http://www.dynamicpatents.com/tag/medtronic/

Goal: Predict vibrational stability of different SMA phases.
Use phonon dispersions to derive thermodynamic properties of each phase.

Technical Details:

High symmetry phase
- Cubic structure w/ 16 atoms
- 2×2×2 supercell = 128 atoms
- 3 independent displacements that break *all* symmetry

Low symmetry phase
- Tetragonal structure w/ 8 atoms
- 2×2×2 supercell = 64 atoms
- 6 independent displacements that break *all* symmetry

Need 9 sets of DFT calculations on 64/128-atom structures with no simplifying symmetry.

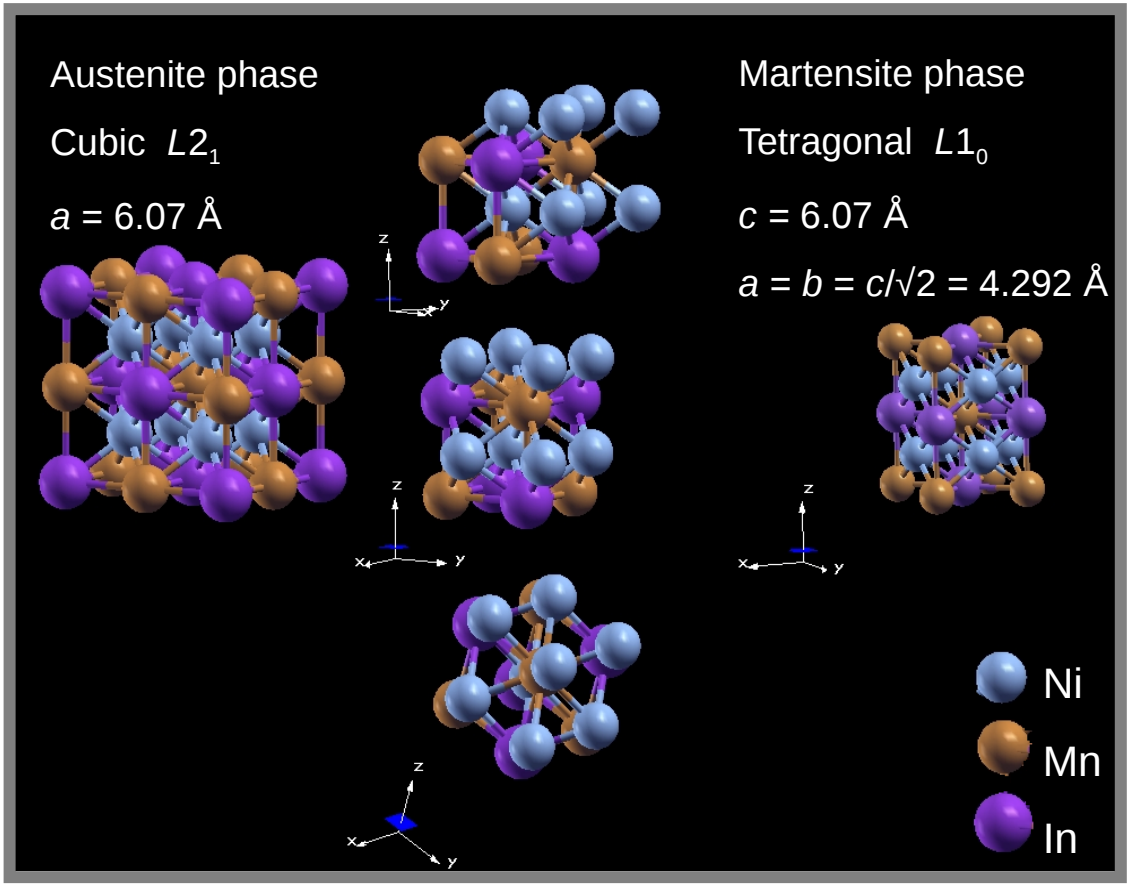

Case Study #1
Magnetic Shape Memory Alloys

Results: Phonon dispersion calculations reveal vibrational instability in high-symmetry SMA phase.

Ni_2MnIn shows same vibrational instability as Ni_2MnGa.

Phonon dispersion of L21 NiMnIn

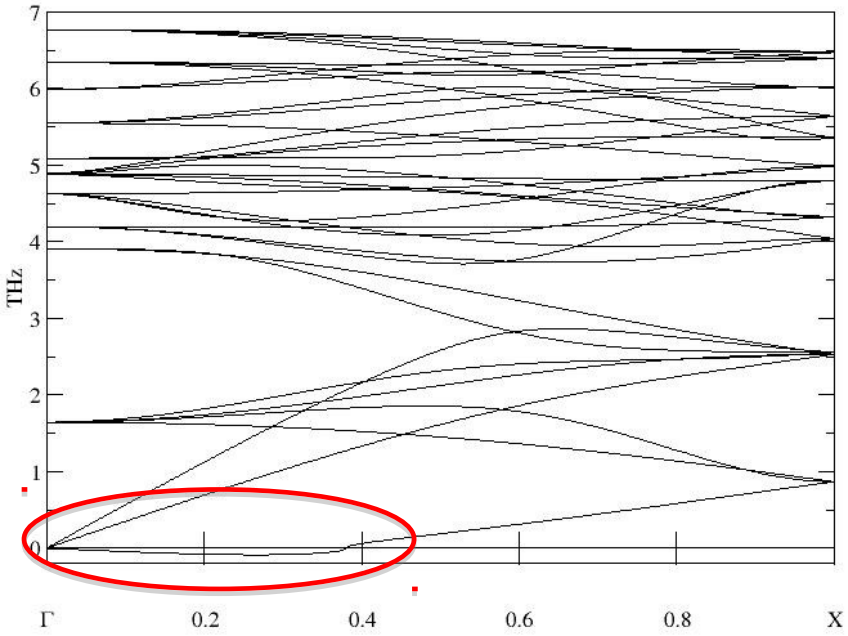

Phonon dispersion of L10 NiMnIn

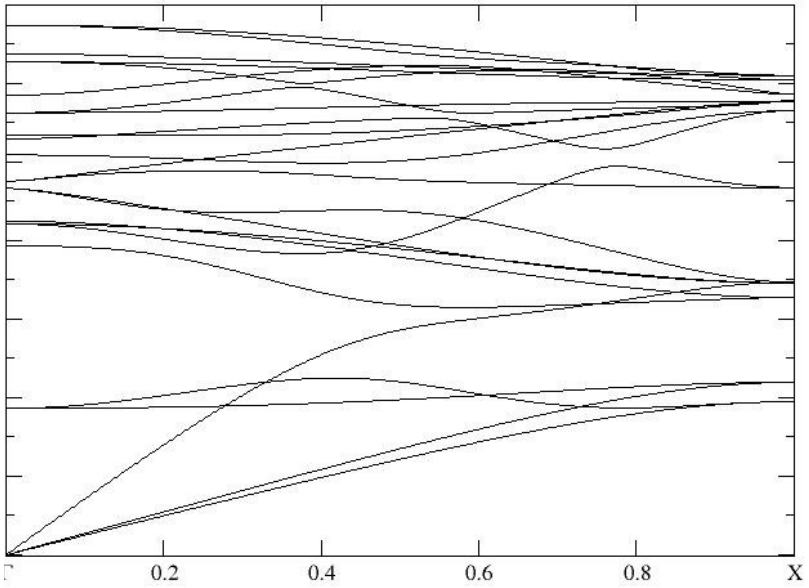

Case Study #1
Magnetic Shape Memory Alloys

Results: Thermodynamics of free energy surfaces show no tetragonal ↔ cubic phase transformation at finite temperatures.

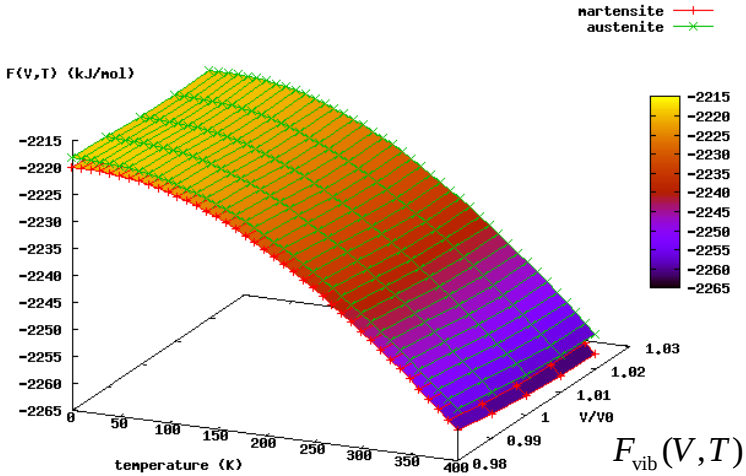

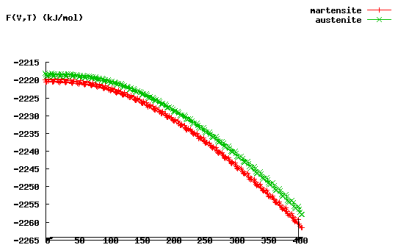

$$F(V,T) = E(V) + F_{\text{vib}}(V,T)$$

$$F_{\text{vib}}(V,T) = k_B T \int_0^{\infty} \ln\left[2\sinh\left(\frac{h\upsilon}{2k_B T}\right)\right] g(\upsilon)\, d\upsilon$$

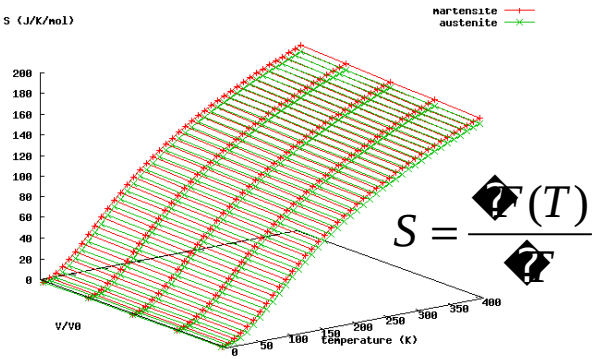

$$S = \frac{\partial F(T)}{\partial T}$$

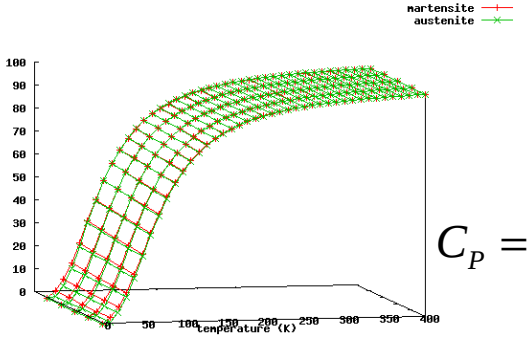

$$C_P = T\frac{\partial S}{\partial T}$$

Case Study #2
Hall Conductivity in Magnetic Metals

Goal: Understand how relativistic effects (i.e. spin-orbit coupling) alter electron population in energy bands.

Technical Details:

- Magnetic iron lattice w/ 2 possible spin states per electron (up or down)
- Spin-orbit coupling makes spin direction-dependent
- Magnetic "vector" on each electron is assigned 3 components

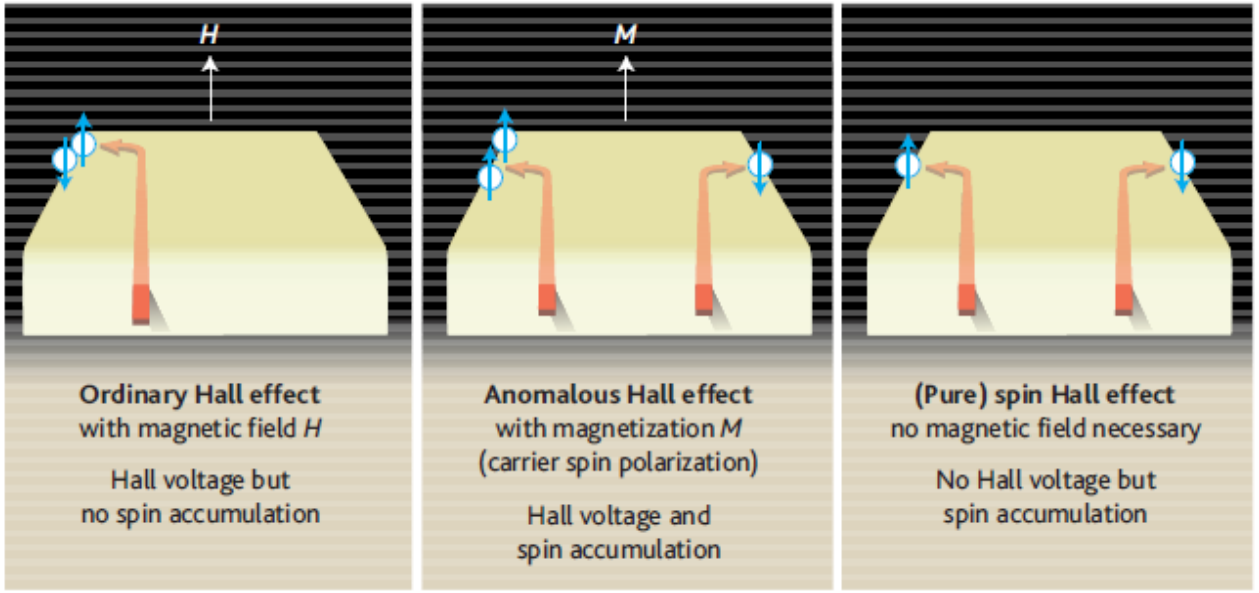

J. Inoue and H. Ohno. *Science*: 309 (2005).

Need to populate iron's 8 valence electrons, each with 3 magnetic degrees of freedom, into 40 energy bands along 4 high-symmetry lines in the 1st Brillouin zone. Numerical precision requires evaluation at 500 points along each line.

Case Study #2
Hall Conductivity in Magnetic Metals

Results: DFT with spin-orbit coupling can generate electronic band diagrams with band “anti-crossings.”

These crossings can be used to estimate the intrinsic contribution to the anomalous Hall conductivity in a ferromagnetic metal.

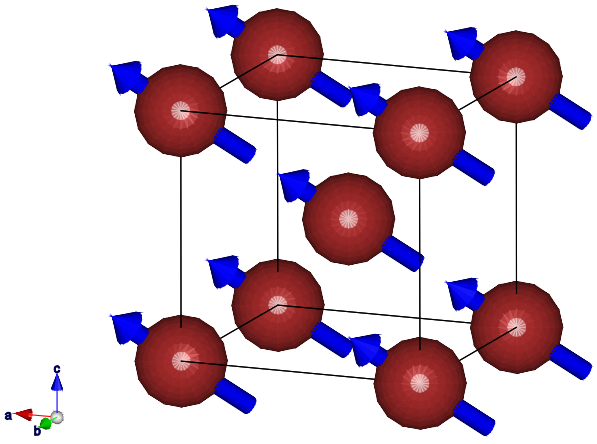

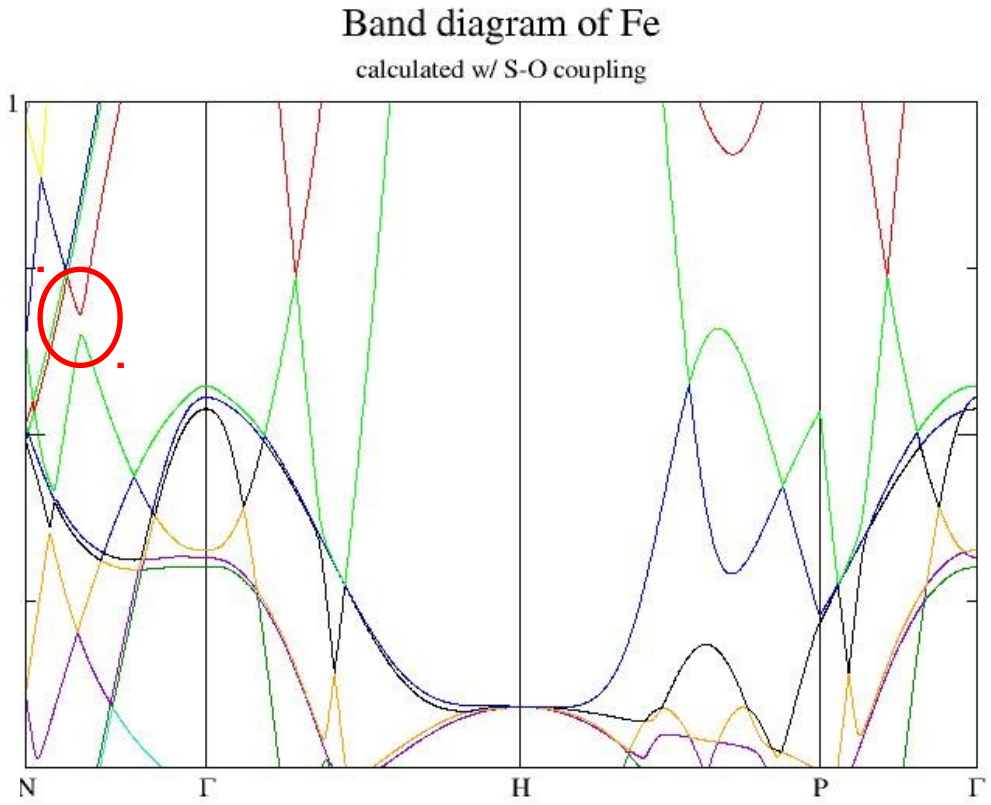

THERMOELECTRIC MATERIALS

Performance: Dimensionless figure of merit ZT

$$ZT = \frac{\sigma S^2}{(\kappa_e + \kappa_L)} T$$

σ : electrical conductivity
κ : thermal conductivity ($\kappa_{electronic}$ + $\kappa_{lattice}$)
S : Seebeck coefficient

Predicting Thermoelectric Performance

Lattice contribution

κ_l

- MD force field fitting to correct phonon dispersion
- Lattice thermal conductivity by Green-Kubo fluctuation-dissipation theory or direct thermal gradient application

Electronic contribution

S, σ, κ_e

- Ground state electronic band structure calculations using density functional theory
- Boltzmann Transport calculations over electronic bands in relaxation time approximation

ThermoElectrics, Performance Criteria: *Figure of Merit*

Problem : Inter-dependence of σ, κ and S through carrier concentration.

$$ZT = \frac{S^2 \sigma}{\kappa} T$$

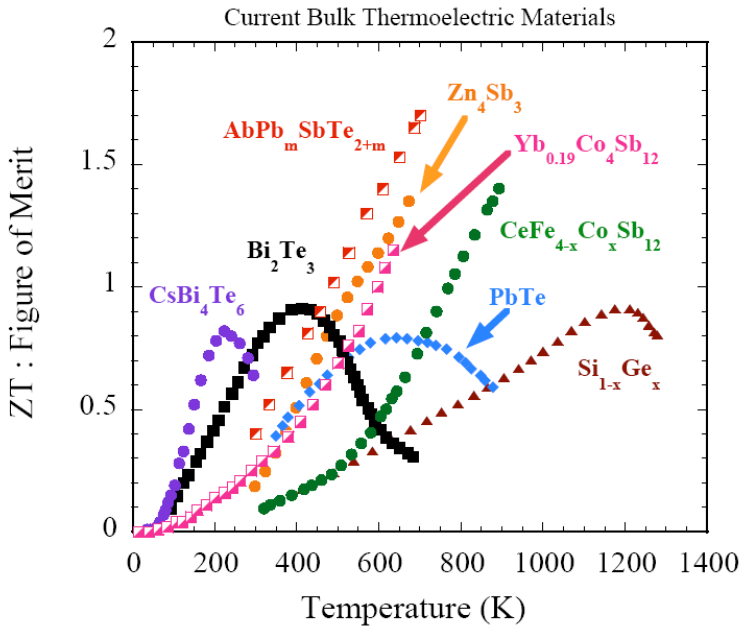

Increasing ZT is difficult - conflicting Properties

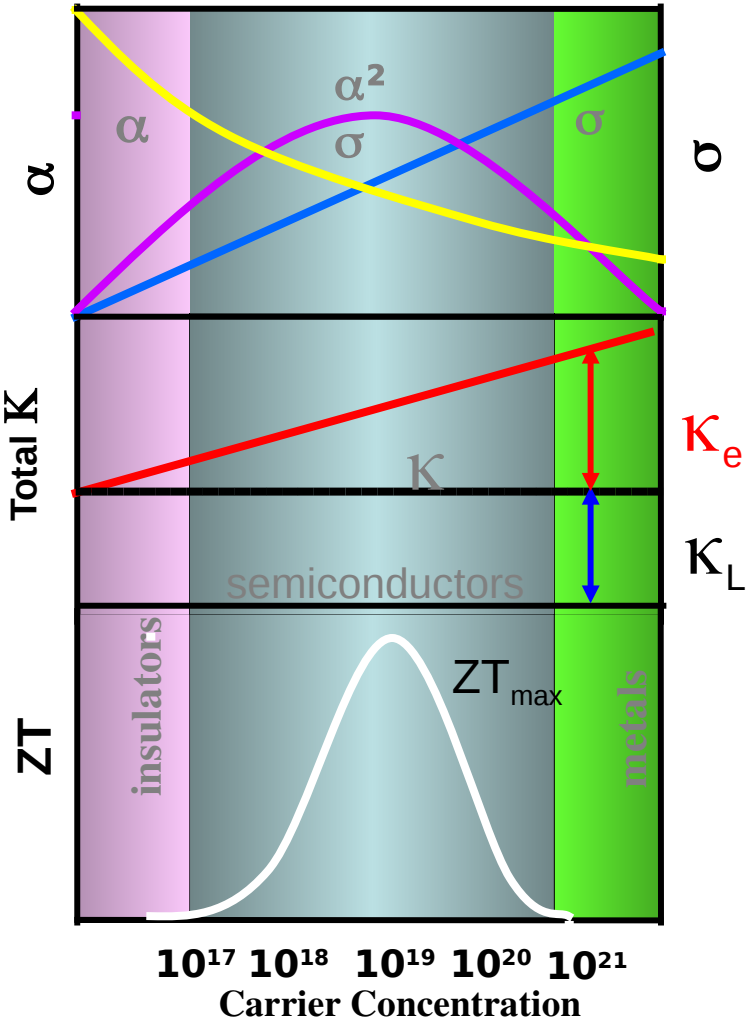

GF Wang and T. Cagin, Appl. Phys. Lett. 89, (2006) 152101

GF Wang and T. Cagin, Phys. Rev. B 75 (2007) 075201

C. Sevik, T. Cagin, in progress

A. Kinaci, C. Sevik, T. Cagin, in progress

Transport Properties From Ab initio Theory

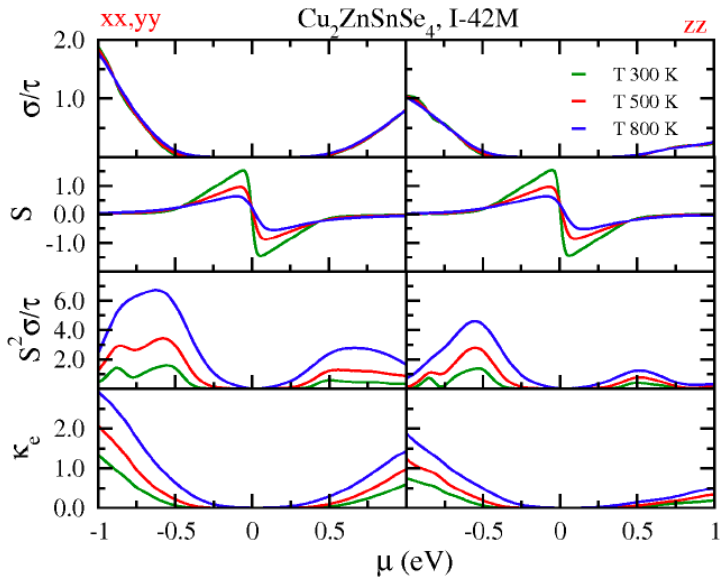

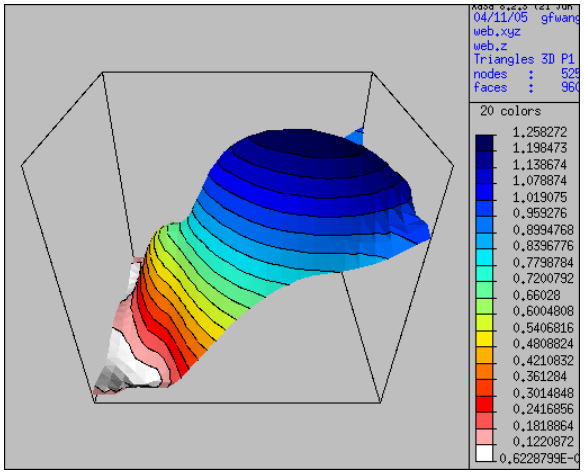

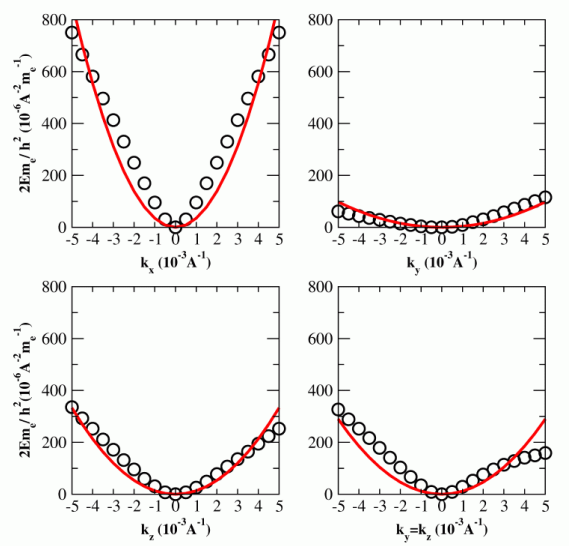

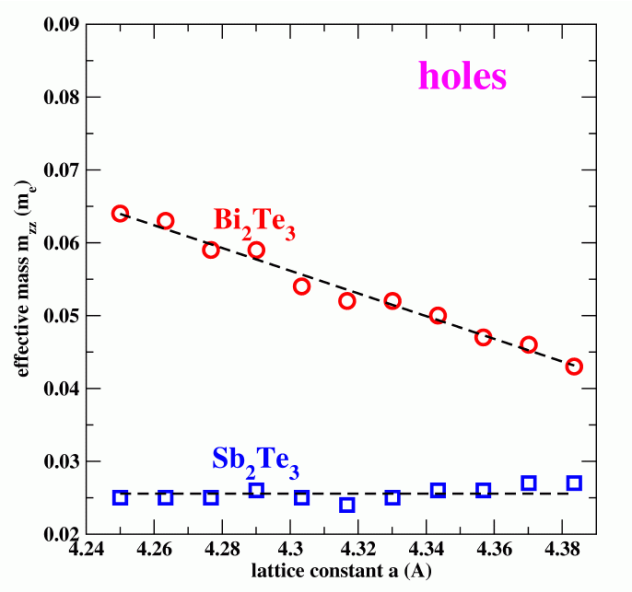

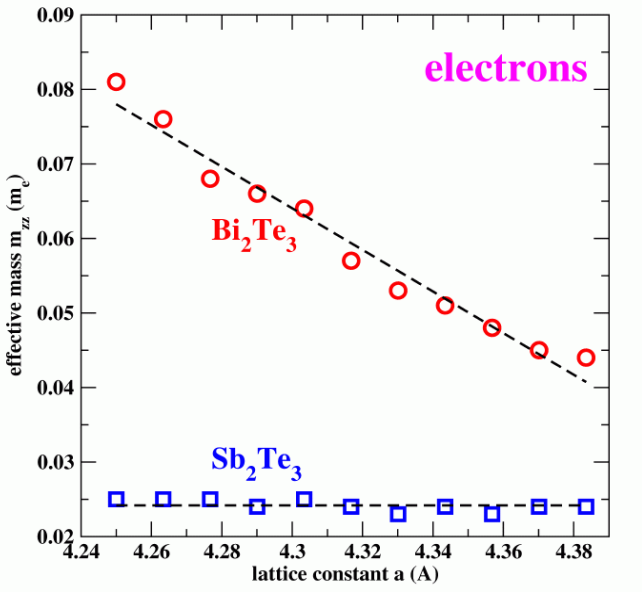

New trends in thermoelectrics: Complex oxides and structural miniaturization (superlattices, nanowire, quantumdots …)

Manipulating properties of $SrTiO_3$

- External stress
- Chemical alloying
- Controlled defects
- Structuring in atomic scale etc…

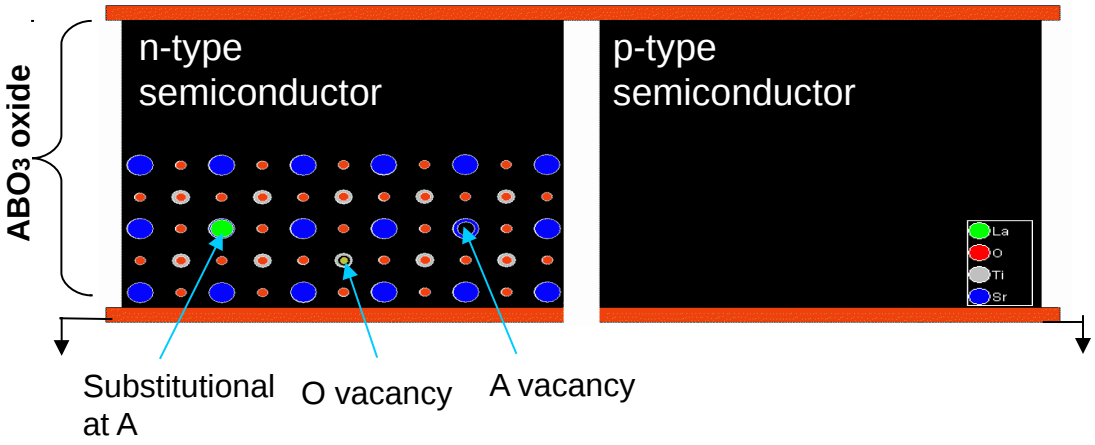

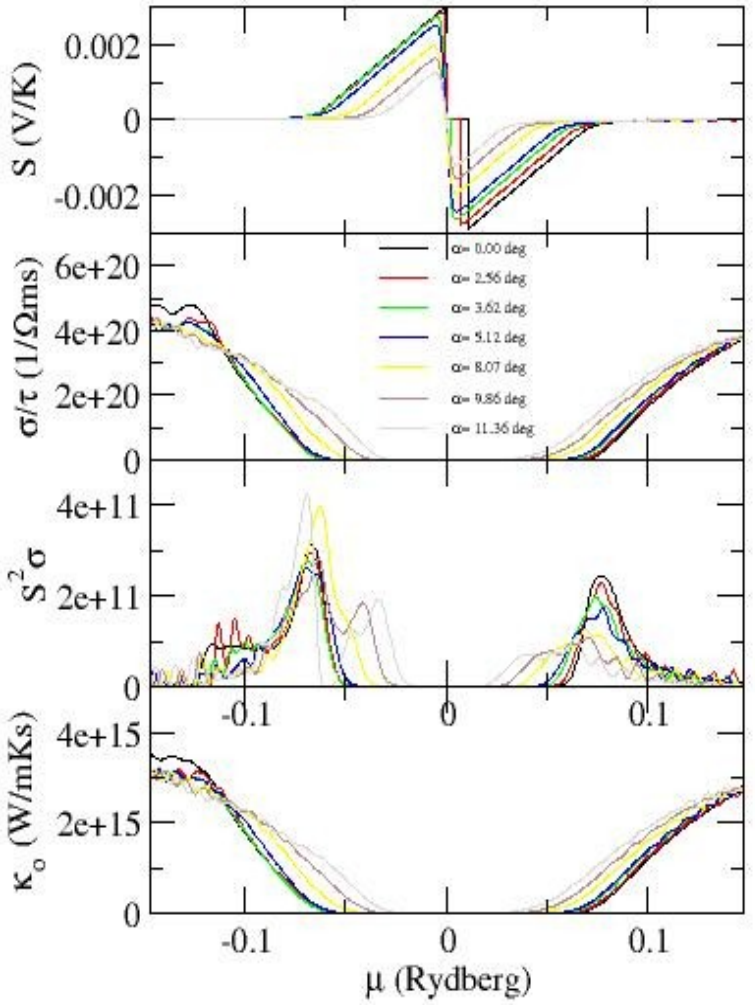

Effect of simple shear on conduction properties of $SrTiO_3$

DFT-BTE STUDIES

Transport Coefficients of La and Nb Doped $SrTiO_3$

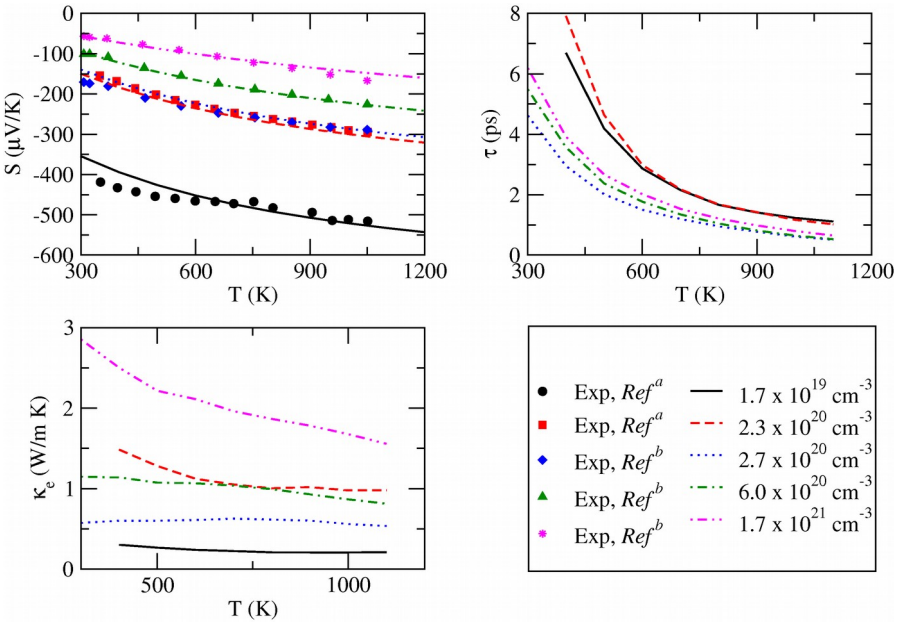

Predicted transport coefficients of La doped SrTiO3 at different La concentrations

[a]Ohta et al. (2005), [b]Muta et al. (2003)

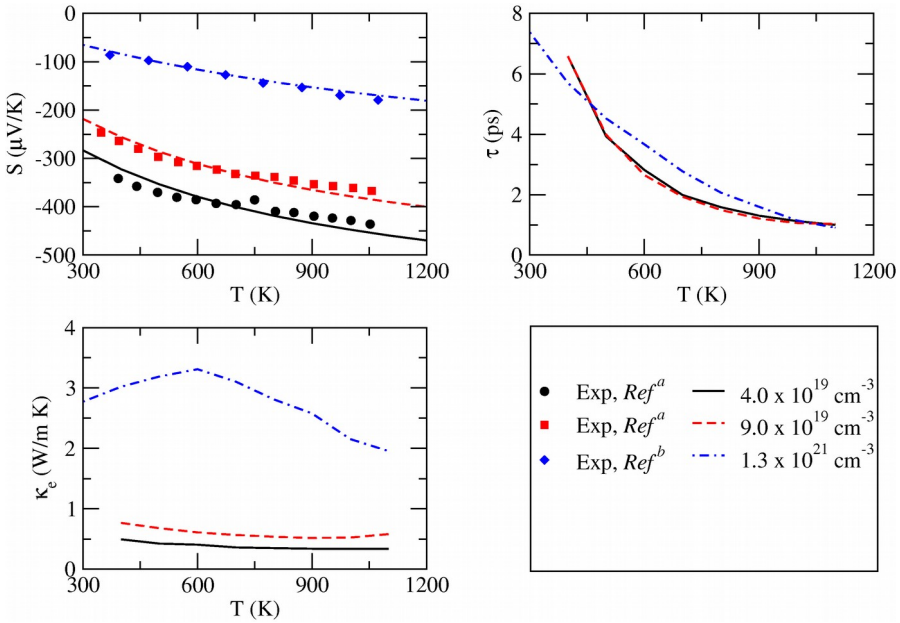

Predicted transport coefficients of Nb doped SrTiO3 at different Nb concentrations

[a]Ohta et al. (2005), [b]Kato et al. (2007)

- Almost perfect match of S-T behavior between experimental and simulation

A. Kinaci, C. Sevik and T. Cagin, "Electronic Transport Properties of SrTiO3 and its Alloys: $Sr_{1-x}La_xTiO_3$ and $SrTi_{1-x}M_xO_3$, M = Nb,Ta", submitted to PRB

Modeling of Thermal Transport
Thermal Management Systems
Thermoelectrics

Develop and Apply molecular level methods for thermal transport.

Molecular Dynamics and Boltzmann Transport Equation based simulation methods are developed, implemented and applied in studying these problem.

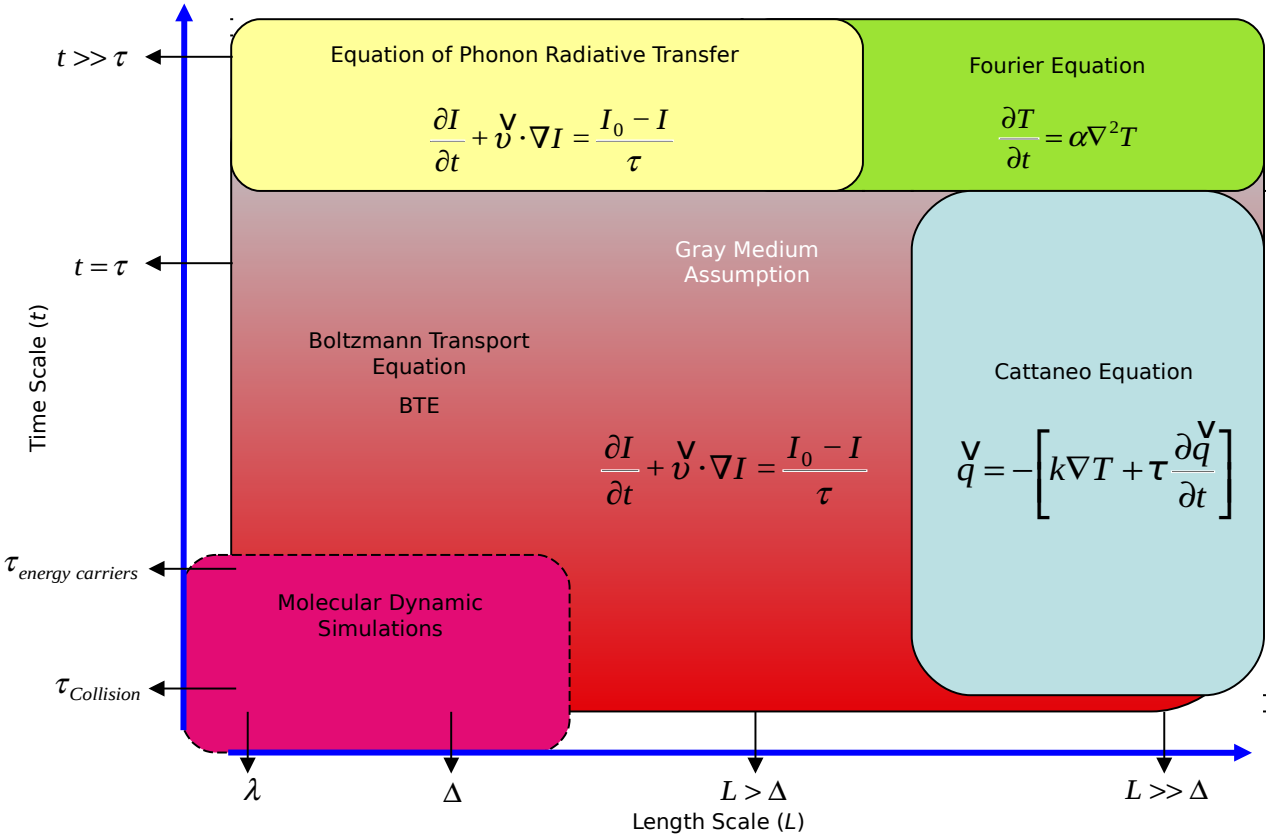

MOLECULAR DYNAMICS STUDIES

Phonon Scattering in Ultra-Thin Superlattices

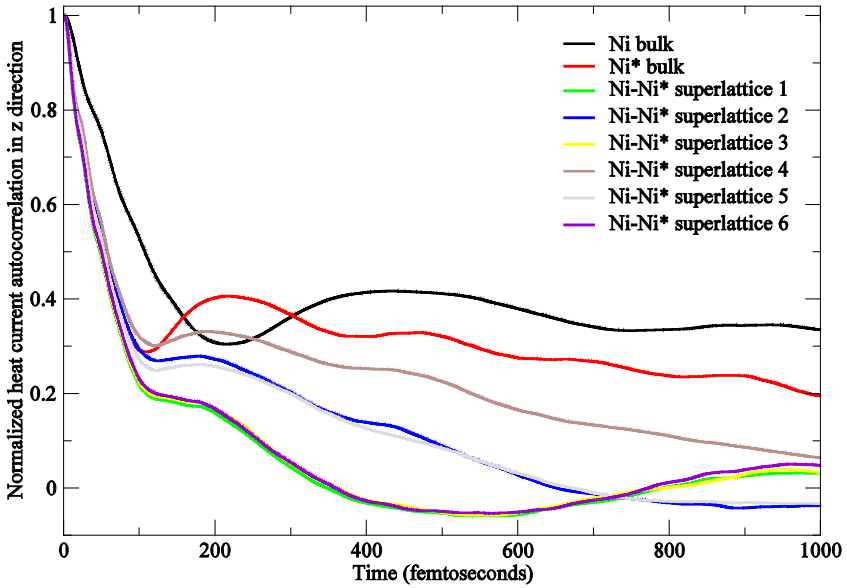

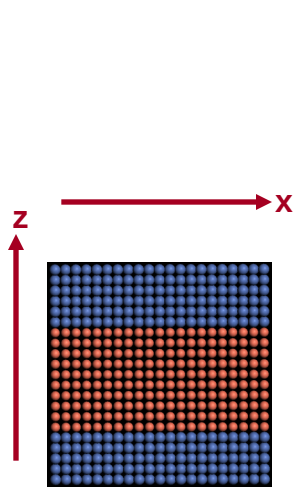

Superlattice 1

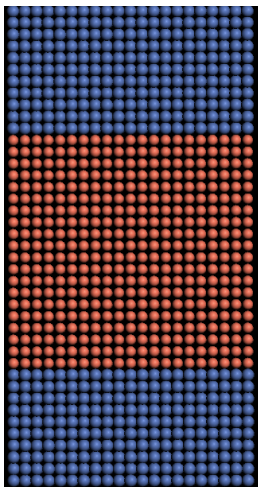

Superlattice 2

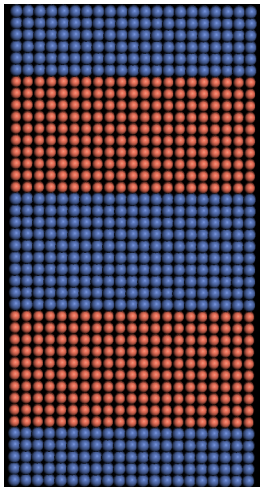

Superlattice 3

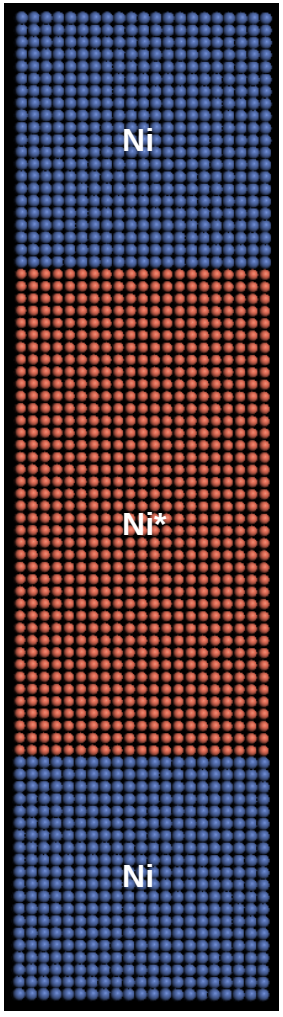

Superlattice 4

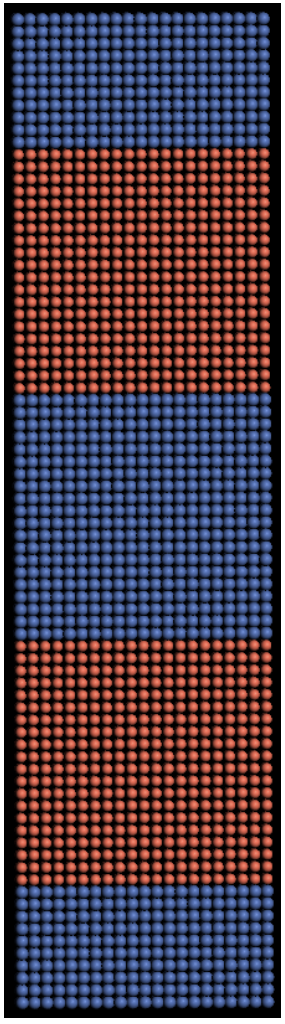

Superlattice 5

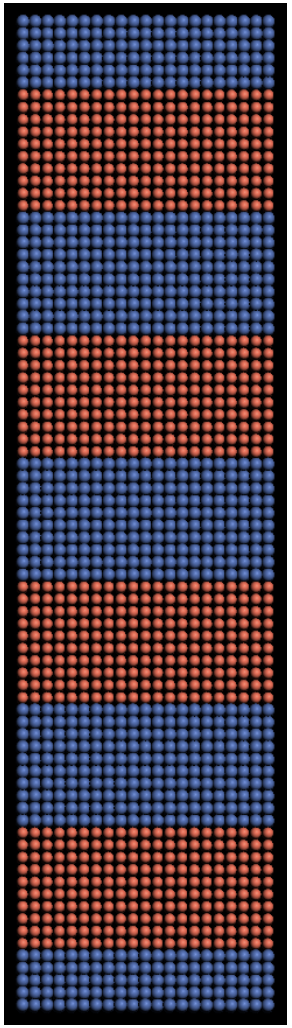

Superlattice 6

Stress-Corrosion Cracking (SCC) in Fe

- Concerns vast range of application
- Combined influence of stress & corrosive environment
- SCC is proved to be connected to GB
  - introduction of impurity element
  - giving no sign of warnings

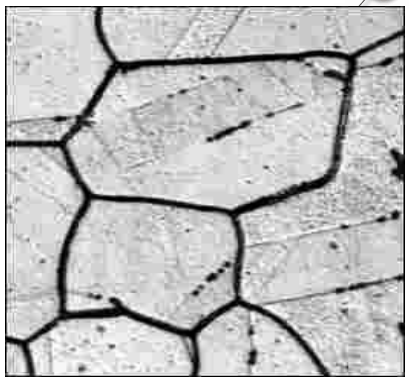

(Source: Corrosion testing lab)

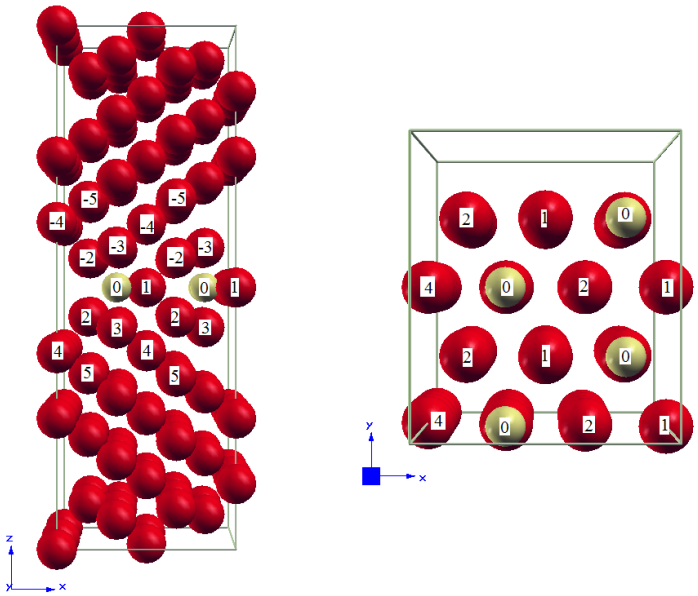

Σ3 (111) grain boundary - 96 Fe atoms

Binding energy

$$E_b N_I = E_{tot}^{GB}(N_{Fe}, N_I) - N_I E_I - E_{tot}^{GB}(N_{Fe}^0) - \frac{N_{Fe} - N_{Fe}^0}{N_{Fe}^0} E_{tot}^{bulk}(N_{Fe}^0)$$

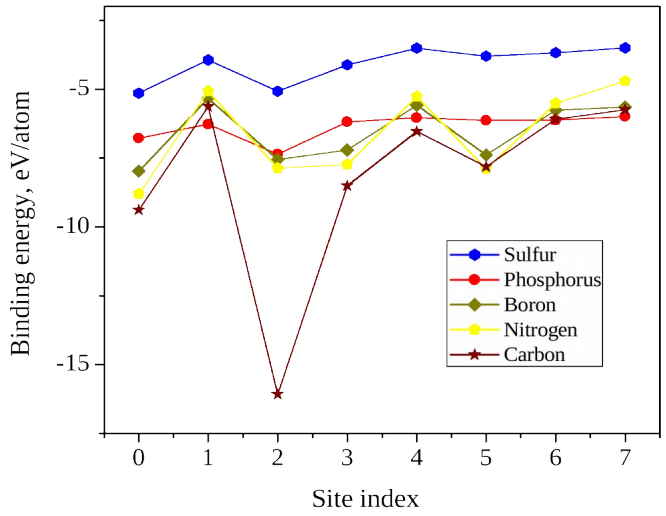

- Carbon ties strongly
- GB0 & GB+/-2 are favorite sites: geometry other than chemistry

Behavior of Sulfur segregation

Fig. Average binding energy of Sulfur as function of layer occupation

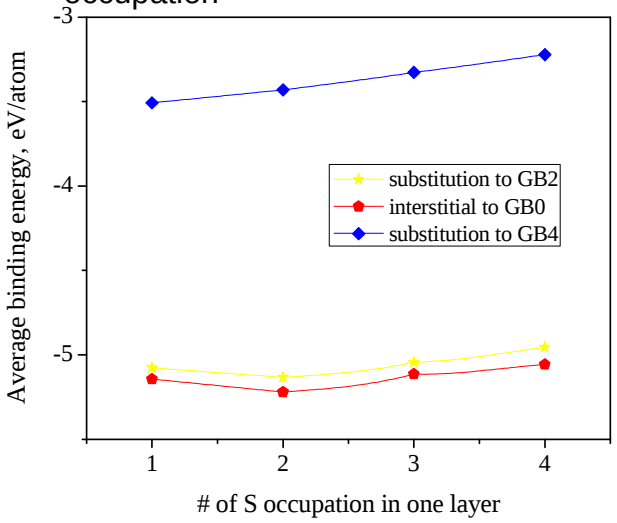

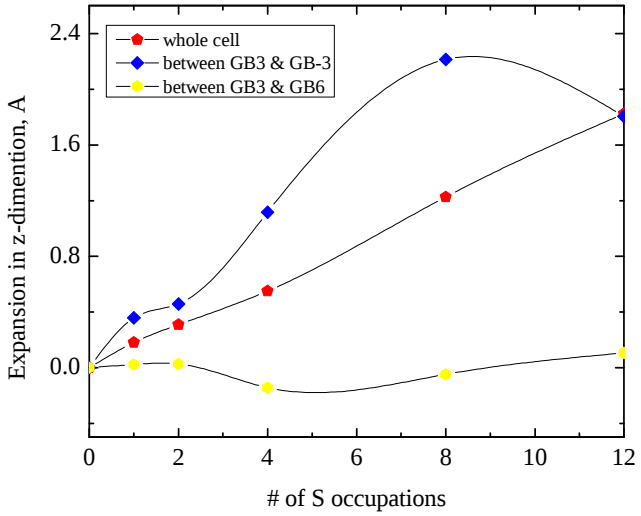

Tab. Behavior of GB cell under S attachment
a, b, c - size of GB cell in x, y, and z dimaentions, respectively
d - distance between GB3 & GB-3

layer	# of occ.	a, Å	b, Å	c, Å	d, Å	- Eb/S, eV
clean cell	0	6.92	7.99	20.29	3.15	--
GB0	1	6.92	8.00	20.47	3.51	-5.14
	2	6.92	8.03	20.60	3.61	-5.22
	3	6.96	8.00	20.75	3.68	-5.11
	4	6.96	8.02	20.84	4.27	-5.06
GB0 & GB2	8	6.89	7.96	22.12	5.36	-4.86
GB0 & GB2 & GB-2	12	6.94	8.02	22.12	4.95	-4.46

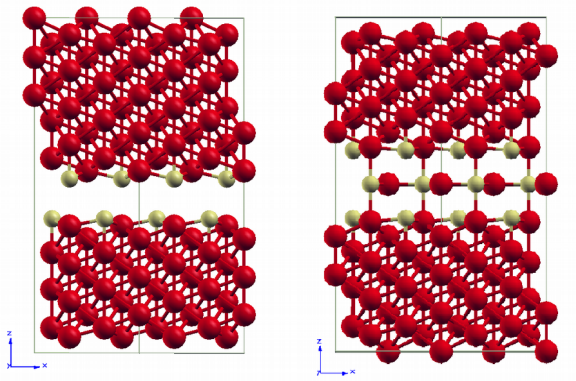

8S 12 S

- z-expansion due to GB separation
- S atoms expose repulsive forces
- interactions around GB broken

Behavior of GB cell under P, N, C and B attachment

Elements	# of occ.	Δa, Å	Δb, Å	Δc, Å	Δd, Å	- Eb/S, eV
P	1	0.00	0.00	0.19	0.34	-6.78
	2	0.00	0.00	0.37	0.45	-7.46
	4	0.01	0.02	0.60	1.15	-7.41
	8	-0.04	-0.06	0.80	1.14	-6.22
	12	0.10	-0.14	1.13	1.25	-5.91
N	1	0.03	-0.01	-0.02	0.29	-8.80
	2	0.02	0.05	-0.03	0.39	-8.95
	4	0.09	-0.01	0.04	0.41	-7.92
	8	0.16	-0.10	-0.08	0.17	-8.15
	12	0.22	-0.21	-0.30	-0.25	-7.74
C	1	0.02	0.00	-0.01	0.25	-9.38
	2	0.02	0.04	-0.02	0.31	-9.40
	4	-0.02	-0.01	0.21	0.56	-8.85
	8	-0.05	-0.05	0.13	0.39	-7.92
	12	-0.19	-0.23	0.53	0.33	-7.42
B	1	-0.01	-0.01	0.08	0.25	-7.98
	2	-0.01	-0.02	0.18	0.27	-7.96
	4	-0.04	-0.04	0.40	0.81	-7.94
	8	-0.07	-0.10	0.20	0.61	-6.98
	12	-0.16	-0.18	0.50	0.52	-6.39

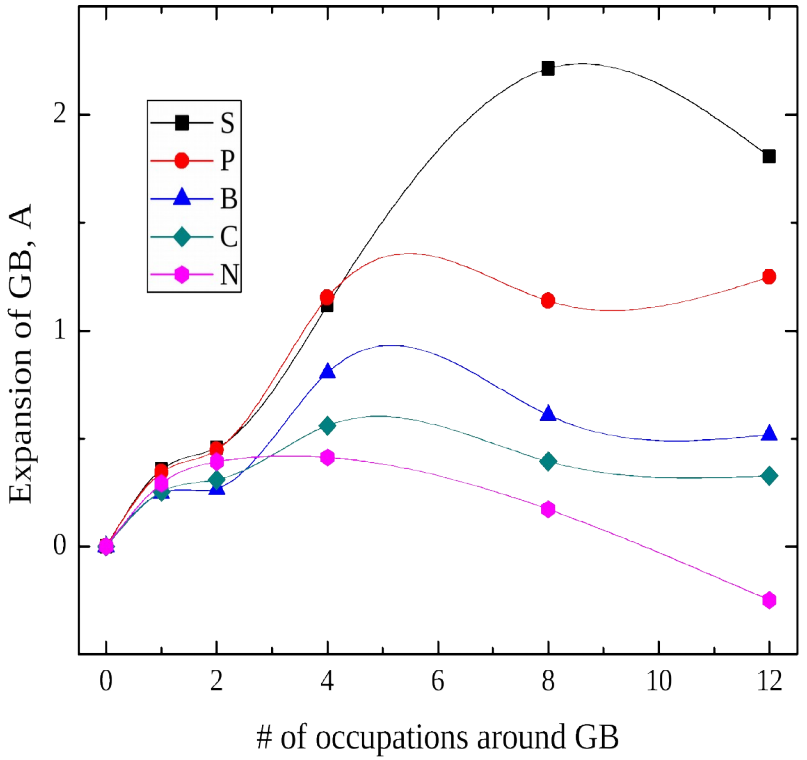

Fig. Comparative separation of Fe Σ3 (111) GB under the attack of different impurity atoms (S, P, N, C, B)

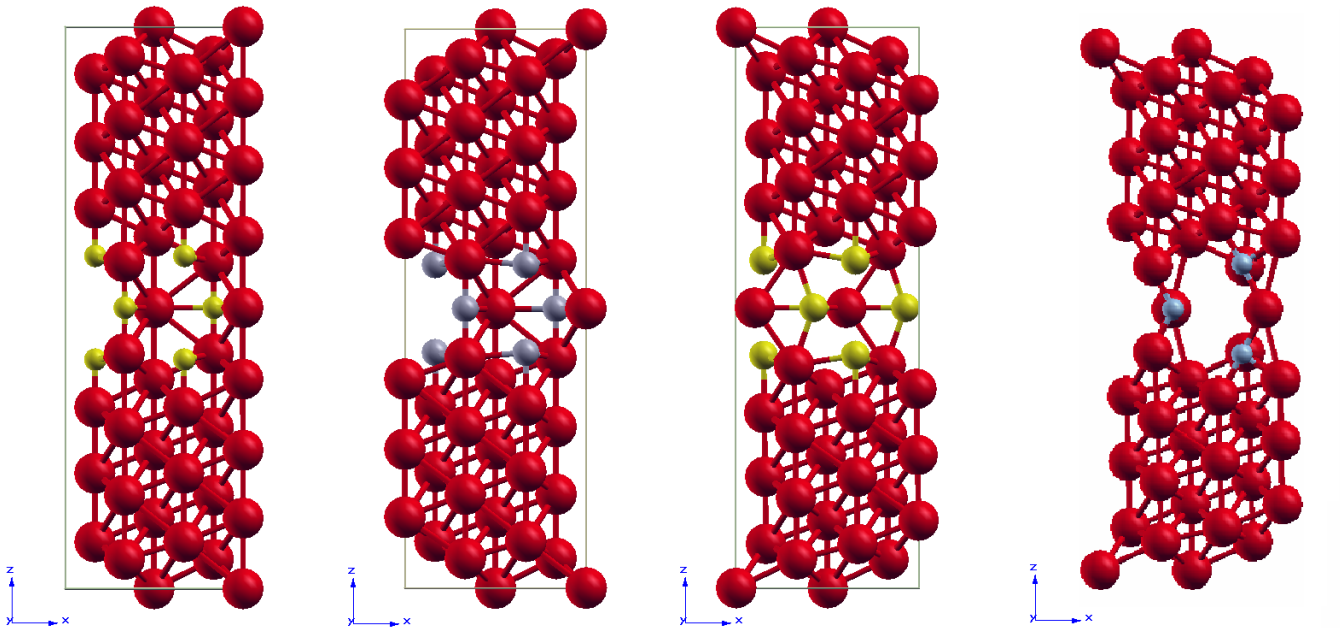

Fig. Behavior of Fe Σ3 (111) GB due to the precipitation of C, B, P and N

- The same binding tendency to a specific locations at GB
- Little interactions from impurity particles on the same layer
- S & P causes the separation of GB, which may initiate cracks
- B & C have little effects on GB mechanical properties
- N weakens the GB structure through formations of cavities and voids

- **First Principles DFT+U studies on (Ce,Th) O2 alloys**
  - Structure, Mechanics, Dynamics, Alloying of CeO2 and ThO2
  - C. Sevik, T. Cagin, “Mechanical and electronic properties of CeO2, ThO2, and (Ce, Th)O2 alloys“ submitted to Phys Rev B. (2009)

Calculated lattice parameters, mechanical properties for CexTh1−xO16.

	a0	B0	C11	C12	C44	Alloy
LSDA+U	5.571	214	379	131	104	Ce1Th7O16
LDA	5.507	216	386	131	95	
LSDA+U	5.548	215	382	132	101	Ce2Th6O16
LDA	5.488	215	385	130	92	
LSDA+U	5.500	213	382	129	96	Ce4Th4O16
LDA	5.448	210	379	126	87	
LSDA+U	5.450	215	386	130	88	Ce6Th2O16
LDA	5.405	209	377	125	79	
LSDA+U	5.425	216	388	130	85	Ce7Th1O16
LDA	5.383	208	376	124	76	

High speed particle impact on atomic scale

- Radiation damage, degradation and embitterment (nuclear material shields, space gadgets etc.)
- Ion implantation, deposition (semiconductor device production)
- Surface modification (surface hardening, corrosion resistance etc.)

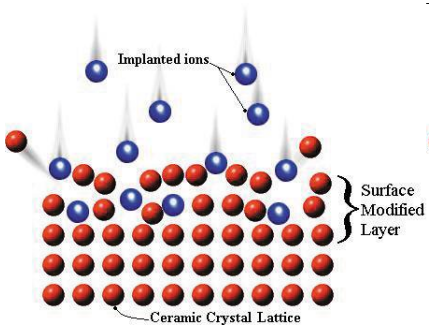

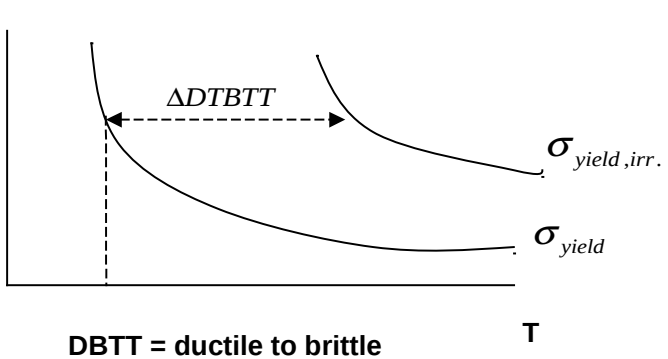

DBTT = ductile to brittle transformation temperature

Molecular Dynamics simulations of irradiation process

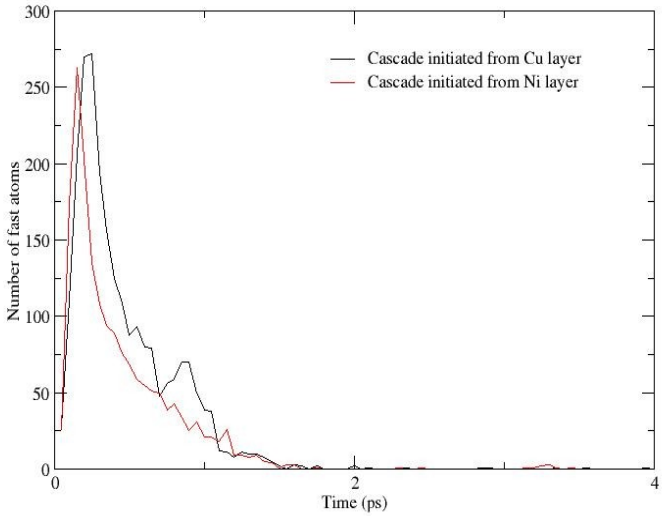

Thermal spike and following thermalization in Cu-Ni superlattice

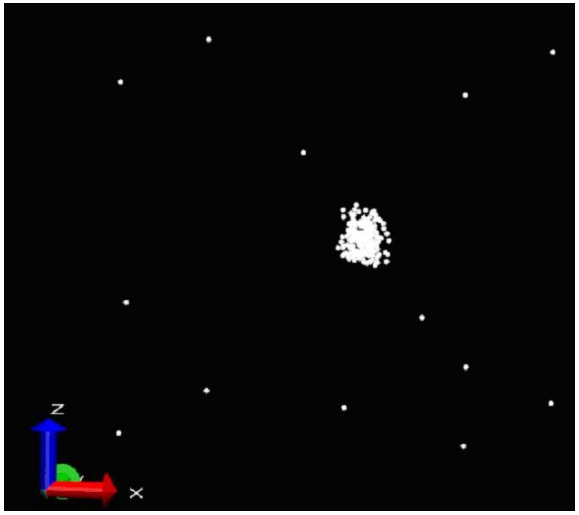

Simulation of microstructure evolution under irradiation in Cu-Ni superlattice

Coarse Grain Molecular Dynamics

- Groups of atoms represented by a single bead
- Used for complex molecules in biosciences (proteins, DNA)
- Used in simulations of entangled polymer melts

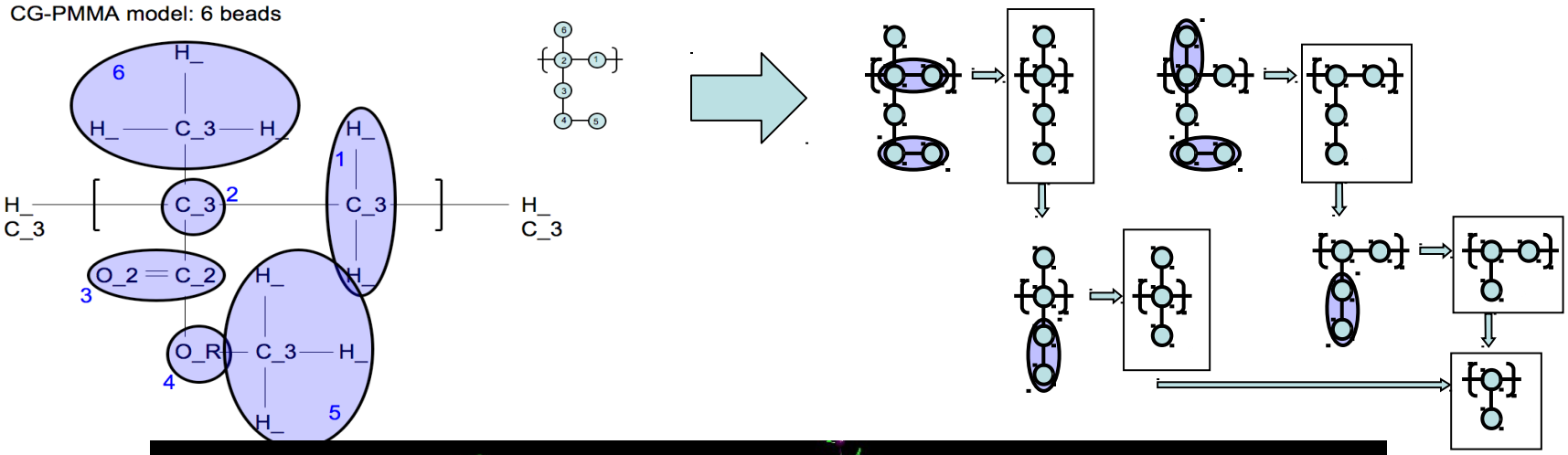

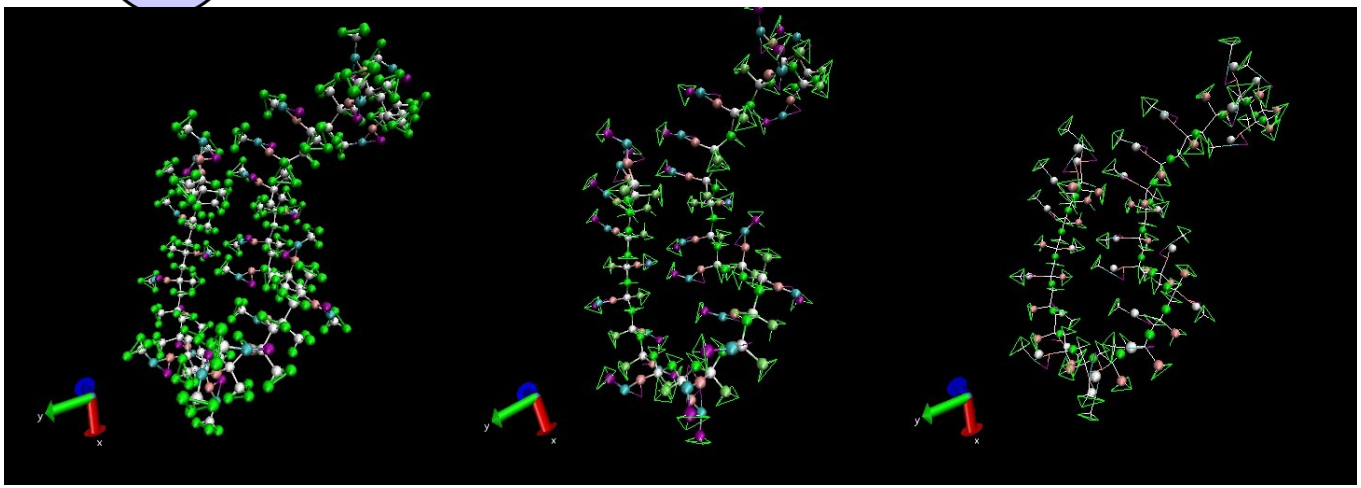

Polyimide-nanotube composites for electro-active materials

A. Chakrabarty, T. Cagin, Polymer J., (2010)

- (ß – CN)APB/ODPA Polyimide
- Piezoelectric polyimide
- Exceptional thermal, mechanical, and dielectric properties
- Amorphous in nature
- Potential use in high temperature application

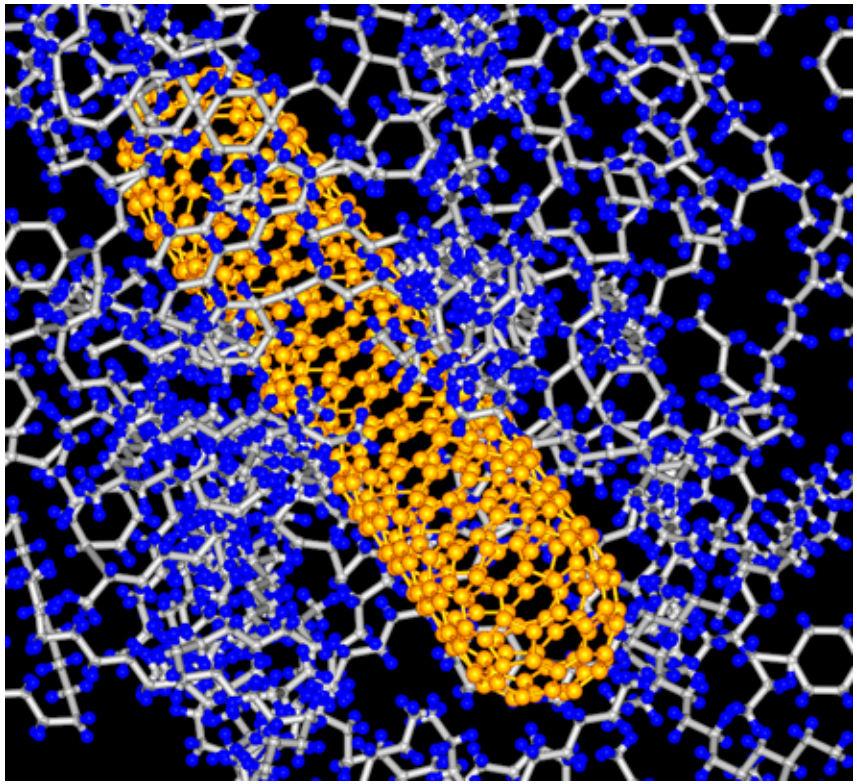

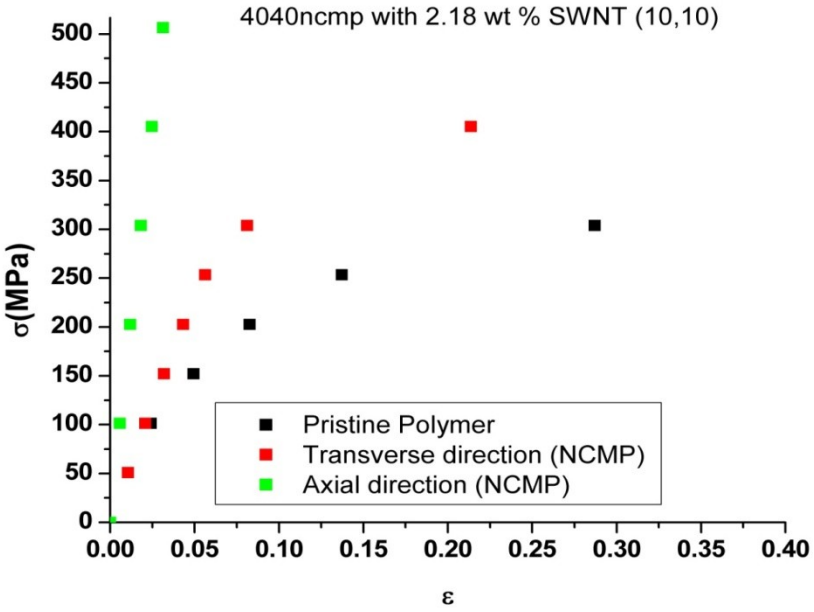
4040ncmp with 2.18 wt % SWNT (10,10)
σ(MPa)
ε
Pristine Polymer
Transverse direction (NCMP)
Axial direction (NCMP)

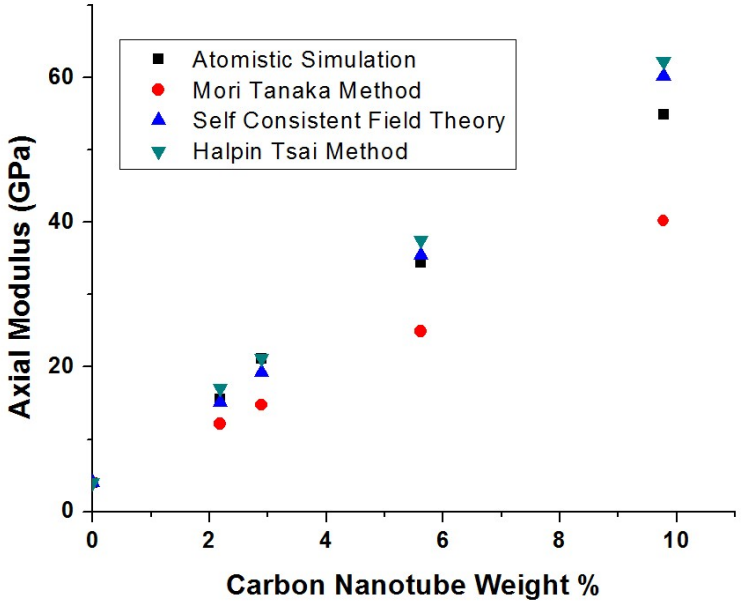
Atomistic Simulation
Mori Tanaka Method
Self Consistent Field Theory
Halpin Tsai Method
Axial Modulus (GPa)
Carbon Nanotube Weight %

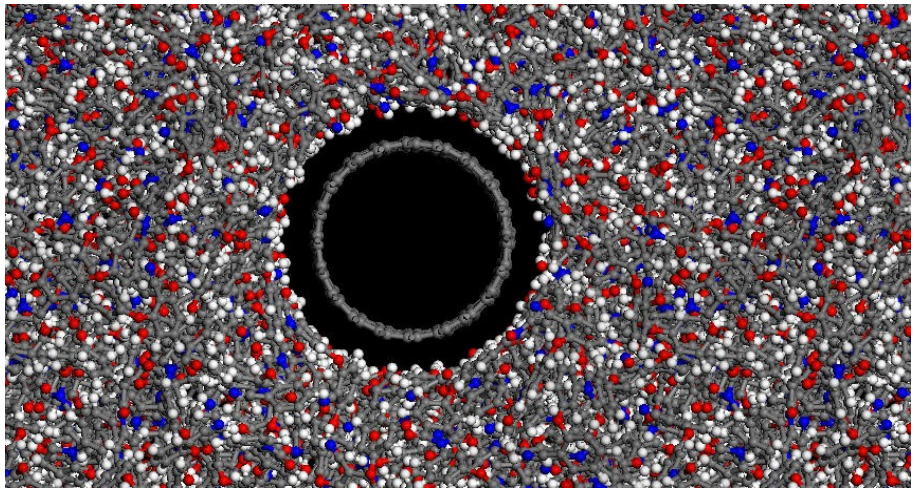

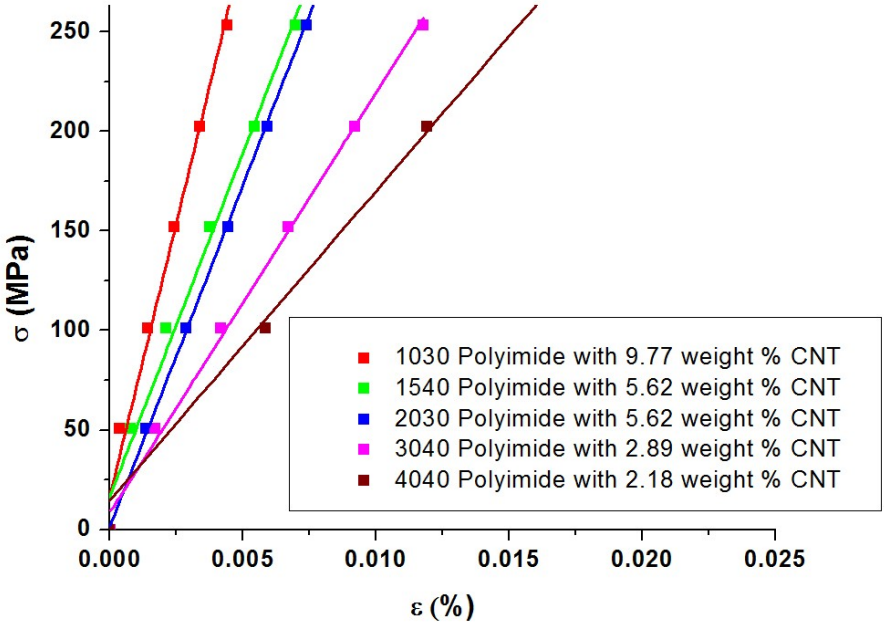
σ (MPa)
ε (%)
1030 Polyimide with 9.77 weight % CNT
1540 Polyimide with 5.62 weight % CNT
2030 Polyimide with 5.62 weight % CNT
3040 Polyimide with 2.89 weight % CNT
4040 Polyimide with 2.18 weight % CNT

Magnetic Shape Memory Alloys -Ni_2MnIn

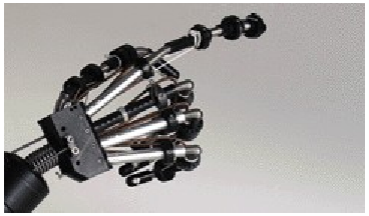

University of Alberta

USAF Aircraft Pictures - http://sun.vmi.edu/hall/afpics.htm

- **Heusler alloy** structure
  - L21 in austenite phase
- Ferromagnetic due to separation of magnetic moments residing on Y atoms
- Ni_2MnGa most extensively studied, with reported recoverable strains ≈10% in the martensite phase

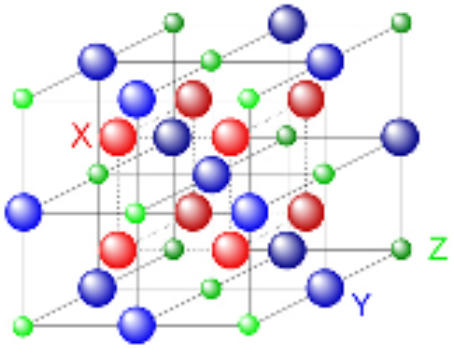

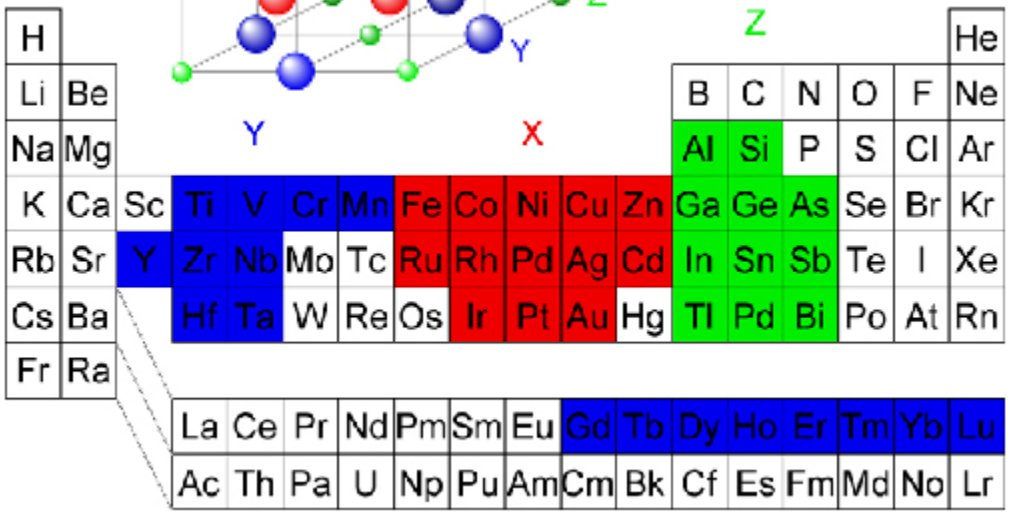

http://www.riken.jp/lab-www/nanomag/research/heusler_e.html

Magnetostructural Coupling in Ni_2MnIn

We apply volume-conserving strains to determine the magneto-mechanical response:

-tetragonal shear

$$\varepsilon = \begin{bmatrix} \delta & 0 & 0 \\ 0 & \delta & 0 \\ 0 & 0 & \dfrac{-\delta^2 - 2\delta}{(\delta+1)^2} \end{bmatrix}$$

-pure shear

$$\varepsilon = \begin{bmatrix} 0 & \delta & 0 \\ \delta & 0 & 0 \\ 0 & 0 & \dfrac{\delta^2}{1-\delta^2} \end{bmatrix}$$